ANNUAL REVIEWS

Annual Review of Fluid Mechanics

Fire Whirls

Ali Tohidi,[1] Michael J. Gollner,[1] and Huahua Xiao[2]

[1]Department of Fire Protection Engineering, University of Maryland, College Park, Maryland 20740; email: mgollner@umd.edu

[2]Department of Aerospace Engineering, University of Maryland, College Park, Maryland 20740

Annu. Rev. Fluid Mech. 2018. 50:187–213

First published as a Review in Advance on October 2, 2017

The *Annual Review of Fluid Mechanics* is online at fluid.annualreviews.org

https://doi.org/10.1146/annurev-fluid-122316-045209

Keywords

fire whirl, tornado, vortex, combustion, vortex breakdown

Abstract

Fire whirls present a powerful intensification of combustion, long studied in the fire research community because of the dangers they present during large urban and wildland fires. However, their destructive power has hidden many features of their formation, growth, and propagation. Therefore, most of what is known about fire whirls comes from scale modeling experiments in the laboratory. Both the methods of formation, which are dominated by wind and geometry, and the inner structure of the whirl, including velocity and temperature fields, have been studied at this scale. Quasi-steady fire whirls directly over a fuel source form the bulk of current experimental knowledge, although many other cases exist in nature. The structure of fire whirls has yet to be reliably measured at large scales; however, scaling laws have been relatively successful in modeling the conditions for formation from small to large scales. This review surveys the state of knowledge concerning the fluid dynamics of fire whirls, including the conditions for their formation, their structure, and the mechanisms that control their unique state. We highlight recent discoveries and survey potential avenues for future research, including using the properties of fire whirls for efficient remediation and energy generation.

1. INTRODUCTION

The fire whirl is one of the most dramatic structures that arises at the intersection of combustion and fluid mechanics. Throughout the literature, fire whirls have been identified by a variety of names, including devil, tornado, twister, whirlwind, or even dragon twist (Japanese). Regardless of the name, when the right combination of wind and fire interact, the result is an intensification of combustion with whirling flames that we call the fire whirl. Although the fire whirl or fire tornado shares some features with its atmospheric counterparts, it remains distinct in its source of buoyancy, combusting fuel, structure, and formation patterns. In nature, fire whirls are most often observed in mass fires. These include both large wildland (also known as forest fires or bushfires) and urban conflagrations, such as the burning of cities or towns. Due to the diversity of topography, wind, and fire conditions that can occur in wildland fires, fire whirls are a frequent phenomenon. **Figure 1** shows a multitude of conditions under which various types of fire whirls are formed. Fire whirls have mostly been studied in the context of fire safety, as their erratic movement and ability to loft burning firebrands contribute to the rapid ignition of new fires, presenting significant hazards to nearby firefighting personnel (Countryman 1971, Forthofer & Goodrick 2011).

Despite the incredible interest they garner, fire whirls remain a relatively poorly understood phenomenon due to their convoluted dynamics and difficulties in obtaining quantitative data (Morton 1970, Albini 1984, Soma & Saito 1991). Hence, many details of fire whirls, whether formed in the laboratory or by natural means, remain elusive. This article reviews the literature on fire whirls, beginning with a description of important parameters governing their dynamics,

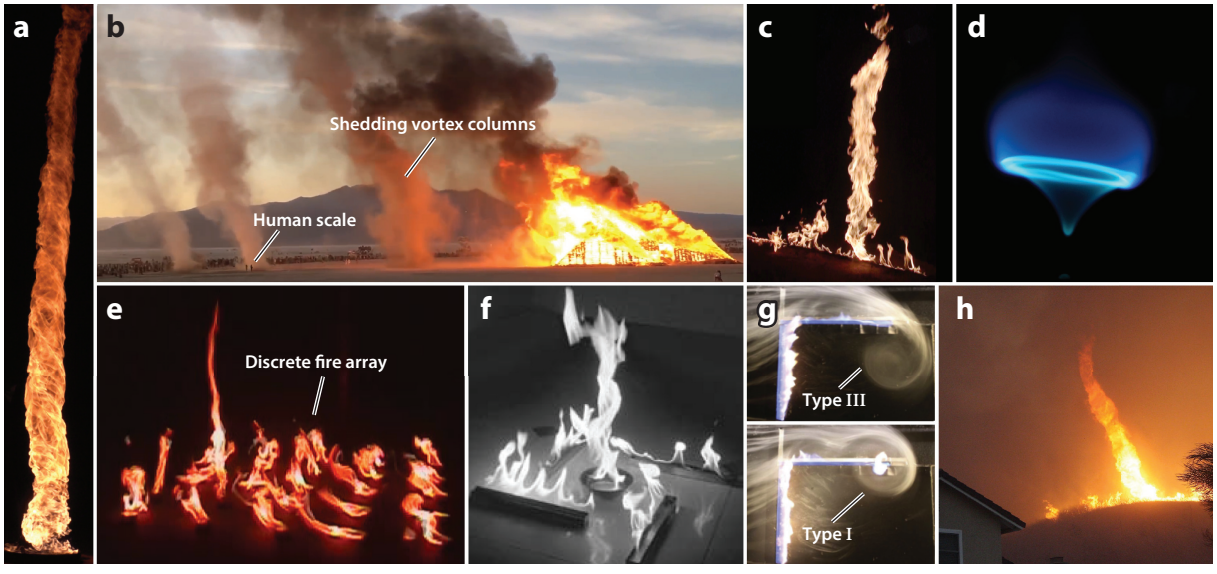

Figure 1

Various forms and scales of fire whirls. (*a*) Full structure of a 30-cm-diameter pool heptane fire whirl in the laboratory at the University of Maryland. (*b*) Shedding columns of whirling hot gases in the wake of a fire plume during the Burning Man event. Photo courtesy of Jeff Kravitz. (*c*) Formation of a fire whirl over a line burner with cross flow (Zhou et al. 2016). (*d*) The blue whirl, thought to form due to vortex breakdown (Xiao et al. 2016). (*e*) Formation of a fire whirl due to the interaction of multiple fire sources with cross flow (Liu et al. 2007). (*f*) Fire whirl formation from multiple fires without wind (Zhou & Wu 2007). (*g*) Generation of whirling columns of hot gases over an L-shaped fire source with 1-cm width through a 0.2-m/s cross flow (Kuwana et al. 2013). (*h*) An inclined fire whirl at the wildland–urban interface during the Freeway Complex fire in Yorba Linda, California, on November 15, 2008. Photo courtesy of David McNew/Getty Images.

followed by a review of the various formation mechanisms and a detailed description of their inner structure. Finally, we review the processes governing the fire whirl, and conclude with avenues for future research.

2. INFLUENTIAL PARAMETERS

Due to fire whirls' high intensity, these destructive forces of nature have primarily been modeled in laboratory-scale experiments. Much knowledge can be gained by examining the governing equations of mass, momentum, and energy and by conducting dimensional analysis on the parameter space. These influential parameters can be summarized as

$$(U_r, U_z, \Gamma, H, \dot{m}) = \Phi\left(L_\mathrm{h}, \dot{Q}, C_\mathrm{p}, \Delta\rho, \rho, \Delta T, T, g, \mu, \beta, \kappa, D_\mathrm{s}\right), \qquad 1.$$

where $\mathbf{U} = (U_r, U_\theta, U_z)$ is the time-averaged velocity vector with radial, azimuthal, and axial components (respectively) in the cylindrical coordinate system, i.e., $(r, \theta, z) \in \mathbb{R}^3$. This coordinate system, with its origin set at the height of the radial boundary layer thickness above the fuel source and its z axis aligned with the (vertical) fire whirl's axis of symmetry, serves as the inertial frame of reference. $\Gamma = \oint_C \mathbf{U} \cdot \mathrm{d}\mathbf{l} = 2\pi r U_\theta$ denotes circulation, H is the flame height, and $\dot{m}$ is the total mass loss (burning) rate of the fuel. L_h denotes a characteristic horizontal length scale. The choice of L_h varies throughout the literature and is often replaced by D_0, which is the pool or burner diameter (Thomas 1963; Emmons & Ying 1967; Soma & Saito 1991; Kuwana et al. 2008; Chow et al. 2010; Lei et al. 2011, 2012; Zhou et al. 2011, 2013) or the horizontal length scale of an obstruction (Kuwana et al. 2007). Alternatively, certain studies take L_h to be the diameter of the whirl (i.e., $D_\mathrm{w} = 2b_\mathrm{w}$) or the spacing/gap size between walls or vanes, depending on the adopted formation configuration in experiments (Hartl 2016, Hartl & Smits 2016). Finally, $\dot{Q}$ is the heat release rate, C_p is the specific heat capacity, ρ is the density, $\Delta\rho$ is the density difference, T is the temperature, ΔT is the excess temperature, g is the acceleration due to gravity, μ is the dynamic viscosity of the gas, β is the coefficient of thermal expansion of the gas, κ is the thermal conductivity of the gas, and D_s is the molecular diffusion coefficient of species.

Applying the Buckingham Π theorem to the parameter space leads to the development of 13 nondimensional groups:

$$\Pi_1 = \frac{U_z}{\sqrt{gH}}, \quad \Pi_2 = \frac{\rho\Gamma}{\mu}, \quad \Pi_3 = \frac{H}{L_\mathrm{h}}, \quad \Pi_4 = \frac{\dot{m}}{\rho\sqrt{gL_\mathrm{h}^5}}, \quad \Pi_5 = \frac{U_r L_\mathrm{h}}{\Gamma},$$

$$\Pi_6 = \frac{\dot{Q}}{\rho C_\mathrm{p} \Delta T\, U_z L_\mathrm{h}^2}, \quad \Pi_7 = \frac{C_\mathrm{p}\mu}{\kappa}, \quad \Pi_8 = \Delta\rho/\rho, \quad \Pi_9 = \Delta T/T, \quad \Pi_{10} = \beta\Delta T, \qquad 2.$$

$$\Pi_{11} = \frac{g\rho^2 L_\mathrm{h}^3}{\mu^2}, \quad \Pi_{12} = \frac{U_r}{U_z}, \quad \Pi_{13} = \frac{\rho L_\mathrm{h} D_\mathrm{s}}{\dot{m}}.$$

Π_1 denotes the Froude number Fr based on the axial velocity component and can be used to indicate the role of buoyancy in the flame structure or formation (Emori & Saito 1982; Grishin et al. 2005; Akhmetov et al. 2007; Kuwana et al. 2007, 2008). Π_2 is the (vortex core) Reynolds number Re based on the azimuthal velocity component (Mullen & Maxworthy 1977), and Π_7 is the flow's Prandtl number Pr. Other nondimensional parameters can be derived using these groups. For instance, the Rossby number Ro, the ratio of nonlinear acceleration to Coriolis acceleration due to rotation, can be obtained from $Ro = (\Pi_3 \times \Pi_5)/\Pi_{12} = U_z H/\Gamma$. The Rossby number can be interpreted to determine critical conditions under which a fire whirl could form (Emmons & Ying 1967, Grishin 2007), and it has been reported that in geostrophic flow with strong circulation (low Ro), the swirling behavior can be better described by Ro than by Fr (Chuah et al. 2011).

It should be noted that the Coriolis force is almost always neglected, as the size of fire whirls is too small compared to the Earth's radius to be significant (Morton 1970, Lei et al. 2015a). Also, the similarity criterion may vary by orders of magnitude for vortices of different scales (Akhmetov et al. 2007). Therefore, the Grashof number, $Gr = \Pi_{10} \times \Pi_{11} = (g\beta\Delta T L_h^3)/\nu^2$, where $\nu = \mu/\rho$, or the Reynolds number may be employed to quantify the similarity. Having obtained Re, Gr, and Pr, one can also define the Richardson and Rayleigh numbers as $Ri = Gr/Re^2$ and $Ra = Gr \times Pr$, respectively. In this context, Ri is the ratio of centrifugal forces to shear forces in a density-stratified field, and Ro is conversely proportional to the swirl number, provided that one neglects the vortex core pressure difference with ambient (Beér & Chigier 1972). However, there are two different mechanisms involved in damping turbulence in fire whirls: cyclostrophic force balance and radial density stratification. Accordingly, Lei et al. (2015b) introduced two simpler definitions of Ri to discuss turbulence suppression. This is discussed in more detail in Section 5.4. Two other important parameters can be derived from Π groups in Equation 2: $\dot{Q}^*$, defined as $\Pi_1 \times \Pi_6 = \dot{Q}/(\rho C_p \Delta T \sqrt{g L_h^5})$, is the ratio of fire power to the enthalpy rate, and Π_4 is the ratio of the fuel-flow rate to the advection rate (Quintiere 2006). Π_{13}^{-1} denotes the Peclet number Pe based on the average velocity of the fuel vapor that leaves its surface (Chuah et al. 2011). This definition of Pe represents the burning rate and has been commonly used in flame height discussions (Chuah et al. 2011, Kuwana et al. 2011, Klimenko & Williams 2013).

Throughout the literature, variations of Π_1 (Fr), Π_2 (Re), Ro, Π_4 (the Froude number of the fuel), and Gr are used to discuss the relative importance of inertial, viscous, rotational, and gravitational forces on fire whirl formation under different ambient and source conditions. Customarily, Π_3 has been adopted as the dimensionless flame height. Following this choice, empirical relations have been established between the dimensionless flame height (Π_3) and Π_1, Ro, Π_4, and Π_{13}^{-1} (Pe). Also, empirical relations exist between $\dot{Q}$ and thermal characteristics of the fire whirl, i.e., the vortex core radius and the plume radius. In addition, variations of $\dot{Q}^*$ ($\Pi_1 \times \Pi_6$) are known to show correlations between the flame height and circulation, which are described later. Other Π groups that are used in obtaining Ra and Ri (particularly Ri) are of significant importance in that they can be used to describe entrainment models, stability, and the turbulent suppression process in fire whirls. However, because the magnitude of the radial velocity is not of the order of other velocity components, Π_5 and Π_{12} thus far have been given less attention in the literature.

3. FORMATION OF FIRE WHIRLS

Fire whirls emerge when terrain/domain features (obstructions) and wind coalesce over a strong, self-sustaining source of buoyancy (fire plume) and form a concentrated flaming vortex column. A fire whirl is not necessarily composed of swirling flames within the vortex column (Countryman 1971), as many cases formed from hot gases downwind of large fires have also been reported (**Figure 1*b***) (Zhou & Wu 2007, McRae et al. 2013). Hence, given the collective body of evidence on fire whirls, they can be classified in two main types: on source and off source. When the whirling flame (vortex column) forms directly over the fuel source, the fire whirl is defined as on source, and when it forms offset from the fuel surface, it is considered off source (Hartl 2016). Both on-source and off-source types can be found in a quasi-steady or unsteady state. In the remaining sections, we use this classification to describe documented instances of fire whirls.

Fire whirls can also be categorized by their characteristic length scale, which is often chosen to be the height of the vortex column. Fire whirls with flame heights between 0.1 and 1.0 m are defined as small scale (Snegirev et al. 2004) and have been abundantly studied both experimentally and numerically (Emori & Saito 1982; Battaglia et al. 2000a,b; Snegirev et al. 2004; Hassan et al.

2005; Zhou & Wu 2007; Chuah et al. 2009; Lei et al. 2015a; Hartl & Smits 2016; Lei & Liu 2016). Whirls with flame heights between 1 and 10 m are categorized as medium scale, whereas whirls of the order of tens to hundreds of meters in height are categorized as large scale (Snegirev et al. 2004, Hartl 2016). Even larger events of the order of kilometers that have occurred during large urban conflagrations (Soma & Saito 1991) or bushfires are documented in the literature. For instance, McRae et al. (2013) described a fire-atmospheric event termed pyro-tornadogenesis.

3.1. Essential Conditions for Fire Whirl Formation

Three factors are essential to the formation of all types and scales of fire whirls: a thermally driven fluid sink, an eddy (vorticity) generation mechanism, and a surface drag force to create a radial boundary layer, which facilitates air entrainment to the generated vortex column (Byram & Martin 1962, 1970). The fire acts as a fluid sink, where the generated plume naturally drives horizontal flows radially toward the vortex column. Therefore, the most substantial element in fire whirl formation is the presence of an eddy-generating mechanism.

During mass fires, there is a large possibility of having strong eddies coalescing with fluid sinks and shear forces at the base. In these extreme events, various natural means exist that can generate the required eddy, such as flows channeled by topological features (Countryman 1971); the interaction of multiple fires or plumes (Liu et al. 2007); the wake of a hill, ridge, or large fire plume (Emori & Saito 1982); and, generally, the transformation of horizontal vorticity into the vertical direction (Church et al. 1980, Forthofer & Goodrick 2011). Examining the definition of vorticity using the Navier–Stokes equations ($\boldsymbol{\omega} = \nabla \times \mathbf{U}$) may provide better insights into the vorticity generation and cascade through the fire whirl domain. Following the notation of Forthofer & Goodrick (2011), the vorticity equation reads as

$$\frac{\mathrm{D}\boldsymbol{\omega}}{\mathrm{D}t} = \underbrace{(\boldsymbol{\omega}\cdot\nabla)\,\mathbf{U} - \boldsymbol{\omega}\,(\nabla\cdot\mathbf{U})}_{\text{Tilting and stretching}} + \underbrace{\frac{1}{\rho^2}\nabla\rho\times\nabla p}_{\text{Baroclinic}} + \underbrace{\nabla\times\left(\frac{\nabla\cdot\hat{\boldsymbol{\sigma}}}{\rho}\right)}_{\text{Traction forces}} + \underbrace{\nabla\times\mathcal{F}_{\mathrm{B}}}_{\text{Body forces}}, \qquad 3.$$

where $\boldsymbol{\omega}$ is the vorticity vector, D is the material derivative, t is time, p is pressure, $\hat{\boldsymbol{\sigma}}$ is the stress tensor due to viscous effects, and $\mathcal{F}_{\mathrm{B}}$ denotes the body forces. The left-hand side of Equation 3 represents the temporal and spatial transport of vorticity throughout the domain. In a fire scenario, the generated vorticity is often transported by the ambient flow. On this note, $(\boldsymbol{\omega}\cdot\nabla)\,\mathbf{U}$ describes the tilting of vorticity due to velocity gradients. This can be directly observed through transitions between horizontal and vertical vortices leading to fire whirl formation (Church et al. 1980, Satoh & Yang 2000). The term $\boldsymbol{\omega}\,(\nabla\cdot\mathbf{U})$ represents the straining effect on the fluid elements due to stretching and/or compressing motions that cause production or dissipation of vorticity. **Figure 2*a*,*b*** illustrates a schematic of this tilting and stretching process in a nonuniform buoyant velocity field where an eddy-generating mechanism exists. Readers are referred to Sharples et al. (2015) and Simpson et al. (2016) for theoretical details on the tilting and stretching of vortices during wildland fire scenarios. The converging flow in the vortex column of a fire whirl also concentrates existing vorticity, as shown in **Figure 2*c***. The baroclinic term represents the generated vorticity due to misalignment between pressure and density gradients (**Figure 2*d***). In fire whirls, a natural misalignment between pressure and density gradients exists (see **Figure 2*d*** and the discussion of Equation 11). In addition, depending on the flow boundary conditions and configurations, the term $\nabla\times(\nabla\cdot\hat{\boldsymbol{\sigma}}/\rho)$ accounts for the viscous diffusion of vorticity due to imposed traction forces on a fluid's elements. **Figure 2*e*** shows a typical vortex tube evolved due to traction forces imposed on the flow by the bottom boundary. Finally, the body forces term in Equation 3 takes into account variations of the vorticity field due to external body forces such as gravity or magnetic

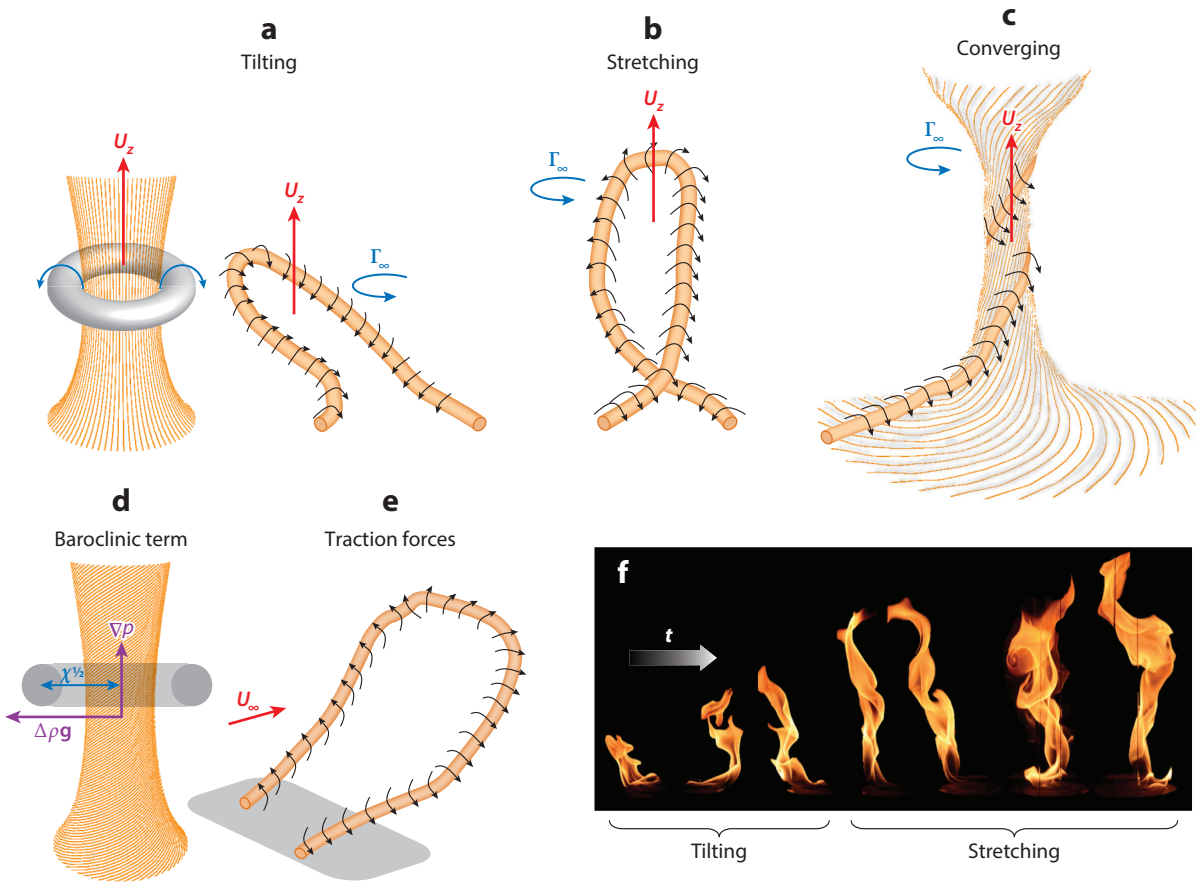

Figure 2

Schematic diagrams of vorticity evolution processes: (*a*) tilting, (*b*) stretching, (*c*) converging, (*d*) the baroclinic term, and (*e*) traction forces evolving the vorticity field. Panel *f* shows the evolution of the flame sheet over time as a pool fire transitions into a fire whirl and demonstrates the presence of tilting and stretching under controlled laboratory conditions.

fields. **Figure 2*f*** shows a schematic of fire whirl development over time where all these effects act together in a complex manner.

The aforementioned conditions are observed in nature or replicated in laboratory experiments under different configurations. A brief summary of documented cases is given below.

3.2. Open Configurations

Most known open fire whirl configurations, including on and off source, quasi-steady and unsteady, can be observed over an L-shaped fire in cross flow, as shown in **Figure 3*a***. This configuration is similar to the Hifukusho-ato fire whirl that occurred following a devastating earthquake in Tokyo in 1923, killing almost 38,000 people (Soma & Saito 1991, Kuwana et al. 2007). Three types of whirls are found in this configuration: stable on-source fire whirls on both ends of the L (type I), unsteady fire whirls that travel along the edges or flanks of the fire and shed periodically in its wake (type II), and a stable off-source whirl that forms within the unburnt region between the L

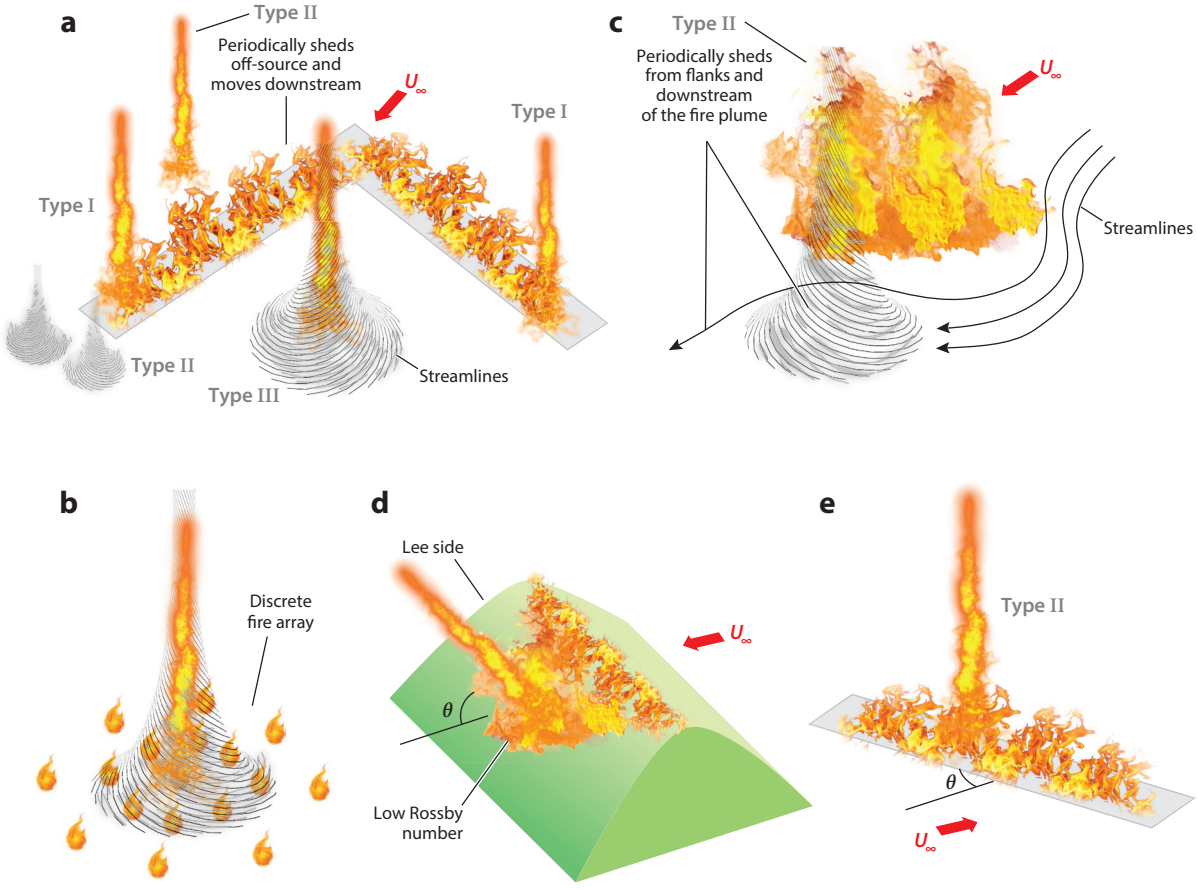

Figure 3

Various open configurations that can generate fire whirls. (*a*) An L-shaped configuration under cross flow, (*b*) a discrete fire array, (*c*) a large fire in cross flow that can shed fire whirls on its flanks or in its wake, (*d*) the lee side of a slope over which an inclined fire whirl can form, and (*e*) a line fire in cross flow. Type I refers to on-source quasi-steady fire whirls, type II encompasses on/off source unsteady (periodic) cases, and type III refers to off-source, stable (quasi-steady) fire whirls that form either with or without the flame.

(type III). Type I whirls are most like the enclosed fire whirls discussed in the following section, as both are on source and quasi-steady. This type could also be formed by an array of multiple fires with or without cross flow (**Figure 3*b***), where any asymmetry in the flow or geometry may cause or amplify the swirl that generates the whirl (Zhou & Wu 2007). This behavior is thought to have been observed following the deliberate firebombing of Dresden and Hamburg during World War II (Soma & Saito 1991). Type II whirls, which are off source and periodic in nature, are seen on the flanks of large wildfires, as well as in the wakes following large, bent-over plumes (**Figure 3*c***). These have been called Dessens fire whirls due to their similarity to whirls observed downstream of a large-scale experiment by Dessens (1962). Finally, type III fire whirls are formed in off-source regions with either flames or merely hot cases under cross flow, similar to the Hifukusho-ato fire whirl described above.

Other fire whirls include those seen on the lee side of a hill following a wildfire (**Figure 3*d***). These whirls are similar to type II or III whirls, depending on whether they are quasi-steady,

the location of the fuel and obstruction, and the orientation of ambient flow. In general, strong vorticity is generated behind an obstruction in cross flow, such as a hill, which has been known to create recirculation regions that can drastically modify fire spread at the tops of hills (Sharples et al. 2015); however, when vorticity tilts upward, one or more fire whirls may form. Fire whirls have also been seen to arise from interactions between a line fire and cross flow (**Figure 3*e***), where an unsteady, on-source whirl can form under specific velocities, orientations, and fire sizes. These fire whirls may travel along a line fire similar to the type II fire whirls that form on the flanks of larger fires (Kuwana et al. 2013, Zhou et al. 2016).

Scale-modeling experiments have revealed, for a variety of configurations, that the formation of fire whirls strongly depends on the velocity of the ambient cross flow. For instance, the formation of a type III fire whirl formed in an L-shaped configuration has been found to depend on a critical cross-flow velocity (Soma & Saito 1991):

$$U_{\mathrm{cr}} = L_{\mathrm{h}}^{3/8} \dot{m}^{1/4}. \tag{4.}$$

An equivalent nondimensional relationship was later proposed by Kuwana et al. (2008) as

$$\frac{U_{\mathrm{cr}}}{\sqrt{gL_{\mathrm{h}}}} \sim Fr_{\mathrm{f}}^{\eta/2}, \tag{5.}$$

where $\eta = 0.3$, $Fr_{\mathrm{f}} = \dot{m}^2/(\rho_\infty^2 g L_{\mathrm{h}})$ is the fuel's Froude number, and ρ_∞ is the air density at ambient temperature. In addition, other correlations between $U_z/\sqrt{gL_{\mathrm{h}}}$ and Fr^η are reported for fire whirls over line fires and type III cases in which the values of η vary (Kuwana et al. 2008, 2013).

3.3. Enclosed Configurations

Because fire whirls in nature are mostly violent and erratic, there are presently no unique parameters that can quantify and describe the necessary formation conditions in open configurations, although some empirical correlations based on dimensional analysis are presented (e.g., Equations 4 and 5). Systematic studies of this nature are carried out in enclosed configurations where either horizontal barriers or mechanical means have been used to induce the required circulation for fire whirl formation. **Figure 4** illustrates schematics of several common enclosed configurations.

Most reported laboratory studies have utilized walls to constrict airflow so that it enters into the test region tangentially. In these configurations, the fuel source is often located at the bottom center of two halves of an offset hollow cylinder (**Figure 4*a***). Hot gases exit the top opening, and ambient air is entrained tangentially into the chamber through the intake(s). As the circulation strength increases, the spiraling flame tilts and eventually elongates so that its axis coincides with the central axis as a sustainable vertical column of whirling flame (Byram & Martin 1962, 1970). This delivers a quasi-steady, on-source fire whirl that has been studied extensively (Satoh & Yang 1996, Satoh et al. 1997, Hassan et al. 2005, Chuah et al. 2011, Hayashi et al. 2011, Kuwana et al. 2011, Lei et al. 2011, Zhou et al. 2013, Dobashi et al. 2015, Hartl & Smits 2016, Wang et al. 2016, Xiao et al. 2016). Square enclosures with tangential slits have also been used (**Figure 4*b***); however, they may introduce redundant eddies into the system due to the recirculation zones at the corners (Hartl & Smits 2016). Others have modified the setup by installing blowers or air intake at the base to provide sufficient air into the chamber (Byram & Martin 1962, 1970; Muraszew et al. 1979) or by using variations with six or more walls (Chuah et al. 2011, Dobashi et al. 2015). **Figure 4*c*** shows a schematic of the setup with an air intake at the base. Using these configurations, the circulation strength and the entrainment can be varied by changing the diameter of the chamber or adjusting the slit spacing.

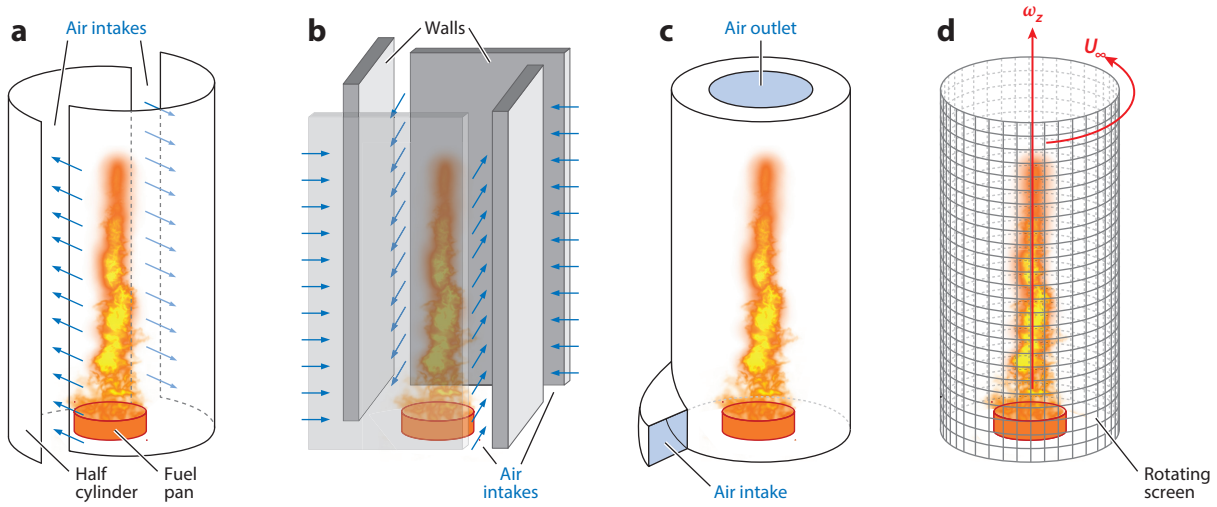

Figure 4

Four types of enclosed configurations for generating fire whirls in the laboratory, including (*a*) two half cylinders offset with slits, (*b*) four walls with slits, (*c*) circular intake, and (*d*) a rotating mesh setup.

Rather than using slits in a solid enclosure, vorticity can also be added to the system via a rotating screen (**Figure 4*d***). This setup has been advantageous in that the circulation strength within the domain can be varied through adjustment of the angular velocity of the screen. Emmons & Ying (1967) first adopted this approach, and as a result, it is often called an Emmons-type fire whirl generator. Because the strength of eddies can be controlled, this approach is favorable for theoretical analysis of the fire whirl structure (Chuah & Kushida 2007), although the domain instrumentation and measurements are more difficult than in fixed-frame setups. This method has also been employed in a series of experiments where multiple equidistant fire whirls were generated between two vertical screens that were both parallel to a propane line fire and moving in opposite directions (Lee & Garris 1969). There are other mechanical methods that can lead to the generation of whirling flames, including the use of air curtains and tangentially oriented blowers at the fuel surface (Byram & Martin 1970, Mullen & Maxworthy 1977, Wang et al. 2015). One advantage of these techniques is that restrictive walls are not necessarily needed, which enables easier experimental probing. However, maintaining the flow symmetry inside the domain is more challenging than with other methods.

While the differences among on-source fire whirls formed in enclosed configurations shown in **Figure 4** are minimal, some differences are observed when the fuel source is changed between a liquid pool fire, a gas burner, or solid combustibles (Hartl 2016, Hartl & Smits 2016). For pool fires and solid combustibles (Martin et al. 1976), the velocity of the gasified vapor is minimal, unlike a gas burner, which may impart additional momentum in the axial direction of the fire whirl, similar to a swirling jet. In a liquid pool fire (Byram & Martin 1962, 1970, Snegirev et al. 2004, Chuah et al. 2009, Kuwana et al. 2011), the swirl establishes an Ekman-like boundary layer over the fuel surface, which draws the flame sheet closer to the fuel surface (Dobashi et al. 2015). This provides more heat to the fuel surface and increases the fuel evaporation and burning rate, subsequently entraining more air (this is discussed in more detail in Section 5.3). There are difficulties characterizing fire whirls over liquid pools, such as the precession of the whirl around the enclosure, uneven heating, and subsequent variations in the heat-release rate. Experimentally,

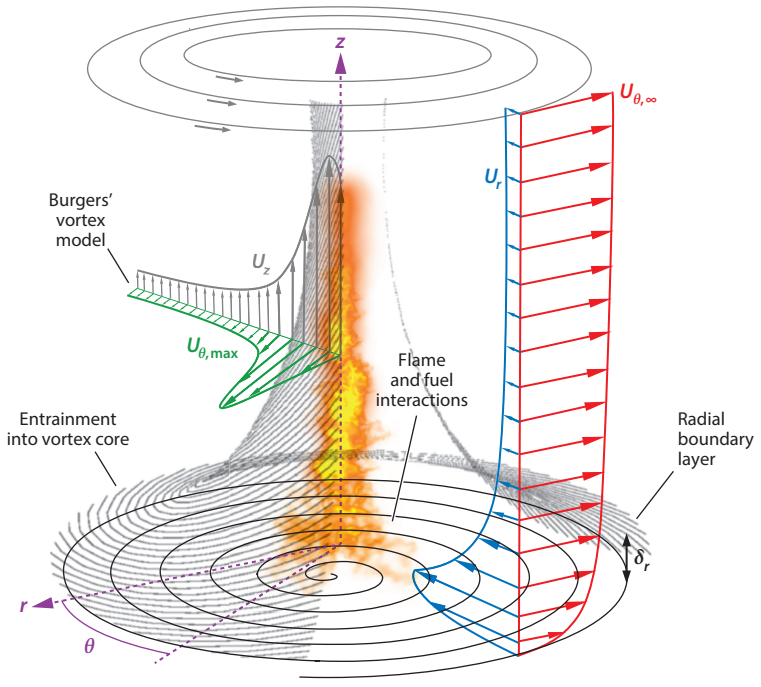

Figure 5

A schematic of the typical velocity field of a quasi-steady, on-source fire whirl.

using a gas burner can be ideal, as the fuel flow rate (fuel's Froude number Π_4) can be set to a constant value during experimentation, decoupling heat release from flow conditions and enabling variations over a wide range. Several works have used gas burners to better understand the empirical relationships between the flame height, ambient swirl, and heat-release rate and have observed that the diameter of the fire whirls generated is somewhat smaller than those generated from liquid pools (Chigier et al. 1970; Beér et al. 1971; Matsuyama et al. 2004; Lei et al. 2015a,b; Hartl 2016; Hartl & Smits 2016).

4. INNER STRUCTURE OF THE FIRE WHIRL

To date, most of what is known about the inner structure of fire whirls comes from the mathematical and experimental characterization of quasi-steady, on-source cases at laboratory scales. The inner structure of such fire whirls can be approximated as a three-dimensional (3D) axisymmetric flow, as shown in a schematic of the velocity field in **Figure 5**.

In order to answer fundamental questions about fire whirls and examine their inner structure, one needs a thorough theoretical model that describes the generated vorticity, velocity, and temperature fields. Although this model does not yet exist, there is a theory of the secondary flow arising from a fluid's rotation over heated solid boundaries, called the Bödewadt (1940) problem, previously considered by Stewartson (1953) and Nydahl (1971). However, there are issues with the stability of the proposed solutions, and fire, which continuously modifies the swirling flow, has not been included in the problem. As for fire whirls, Emmons & Ying (1967) applied turbulent plume theory to a modified model of a free vortex over a ground plane, i.e., 3D

axisymmetric flow. In this section, the vorticity field is first described, followed by a geometric characterization of the structure. Then, the velocity field and thermal composition of fire whirls are described.

4.1. Vorticity Field

Experimental measurements for both small-scale (Emmons & Ying 1967, Soma & Saito 1991) and medium-scale (Muraszew et al. 1979, Lei et al. 2011) enclosed fire whirls reveal that the azimuthal velocity U_θ increases linearly with radius inside the whirl column (vortex core) and decreases proportional to $1/r$ outside of it. This indicates that the fire whirl core can be approximated as a rotating solid body, and outside of the core the flow field is approximately a free vortex. This is further confirmed by particle image velocimetry (PIV) (Matsuyama et al. 2004, Hassan et al. 2005, Akhmetov et al. 2007) and stereo-PIV measurements (Hartl & Smits 2016, Wang et al. 2016). With respect to the vorticity field, other experimental results by Lei et al. (2015b), conducted in a fixed-frame, four-walled enclosure, suggest that the fire whirl domain can be divided into three distinct regions: From the center of the whirl in the radial direction, these include the vortex core, the quasi-free vortex, and the near-wall regions. The first two vorticity zones were previously identified, whereas the near-wall zone forms due to the experimental configuration, according to Lei et al. (2015b). The near-wall zone is rich in vorticity, which conserves the vorticity content of the whirl column by imparting eddies of different scales into the whirl, primarily through the radial inflow boundary layer at the base.

Prior knowledge of the vorticity field delivers a better understanding of the velocity distribution in the domain. Hence, some studies (Byram & Martin 1962, Hassan et al. 2005) adopt the Rankine vortex model (Batchelor 1953, 2000; Kundu et al. 2004) to describe the velocity field of the fire whirl, whereas others (Chuah et al. 2009; Kuwana et al. 2011; Lei et al. 2011, 2015b) report that the Burgers (1948) vortex model best fits their observations. Moreover, Chuah & Kushida (2007) used the Sullivan vortex model (Donaltson & Sullivan 1960) to describe the velocity components of the fire whirl. Assuming that Γ_∞ is the ambient circulation and b_w is radius of the vortex (whirl) core, Equations 6 and 7 show the radial profile of the azimuthal velocity U_θ along with the associated circulation $\Gamma(r)$ for the Rankine (Kundu et al. 2004) and Burgers (1948) vortex models, respectively:

$$U_\theta(r) = \begin{cases} \left(\frac{\Gamma_\infty}{2\pi b_w^2}\right) r, & r \le b_w \\ \left(\frac{\Gamma_\infty}{2\pi}\right) \frac{1}{r}, & r > b_w \end{cases}, \qquad \Gamma(r) = \begin{cases} \left(\frac{\Gamma_\infty}{b_w^2}\right) r^2, & r \le b_w \\ \Gamma_\infty, & r > b_w \end{cases}, \tag{6.}$$

$$U_\theta(r) = \frac{\Gamma_\infty}{2\pi r}(1 - e^{-r^2/b_w^2}), \qquad \Gamma(r) = \Gamma_\infty(1 - e^{-r^2/b_w^2}). \tag{7.}$$

In Burgers' representation (Equations 7), the maximum value of the azimuthal velocity U_θ occurs at $r \approx 1.12091 b_w$ (Kundu et al. 2004, Hartl 2016). **Figure 6*a*** compares the distribution of azimuthal (tangential) velocity with respect to the distance from the vortex column's centerline axis for different vortex models against stereo-PIV measurements made by Hartl (2016) and Hartl & Smits (2016).

Even though some studies (Hayashi et al. 2011, Klimenko & Williams 2013) reported that the Burgers vortex model does not provide an adequate description for the radial distribution of the azimuthal velocity, the available evidence collectively suggests that the Burgers model is the best fit for a quasi-steady, on-source fire whirl (Lei et al. 2015b, Hartl 2016, Hartl & Smits 2016, Wang et al. 2016).

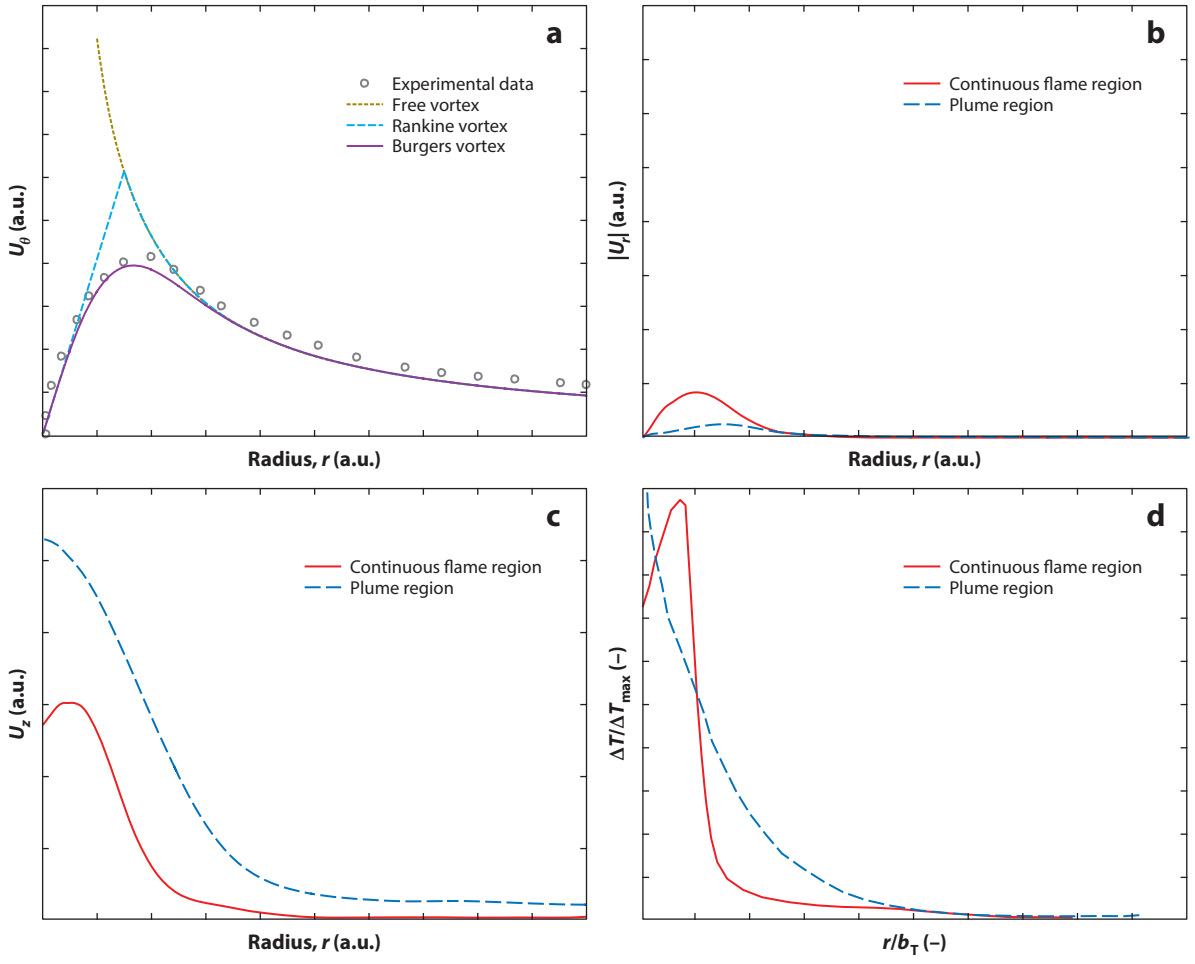

Figure 6

Velocity profiles predicted and measured for the inner and outer structure of an on-source, stationary fire whirl. (*a*) Azimuthal velocity U_θ as a function of radius r, including theoretical predictions and experimental data made by Hartl (2016) and Hartl & Smits (2016). (*b*) Radial velocities $|U_r|$ within the continuous flame and plume regions. (*c*) Axial velocities U_z measured within the continuous flame and plume regions by Hartl (2016). (*d*) Normalized excess temperature $\Delta T/\Delta T_{max}$ measured against normalized radial distance r/b_T, with b_T measured within the continuous flame and plume regions by Lei et al. (2015b).

4.2. Geometric Characteristics

Before further discussion of the velocity field and variation of other parameters, it is important to define the geometric characteristics of the fire whirl in the vertical (z) and radial (r) directions.

4.2.1. Along the z direction. Three distinct regions have been defined along the z direction: the continuous flame, the intermittent flame, and the plume regions (Lei et al. 2013, 2015b). **Figure 7** shows a schematic of these regions. The continuous region represents the fire whirl's core height where the axial flow accelerates upward to the maximum axial centerline velocity. This is observed to occur at $z/H = 0.7$, where H is the time-averaged luminous flame height of the fire whirl (Zukoski et al. 1981, Lei et al. 2013, 2015b). The height of the continuous flame region

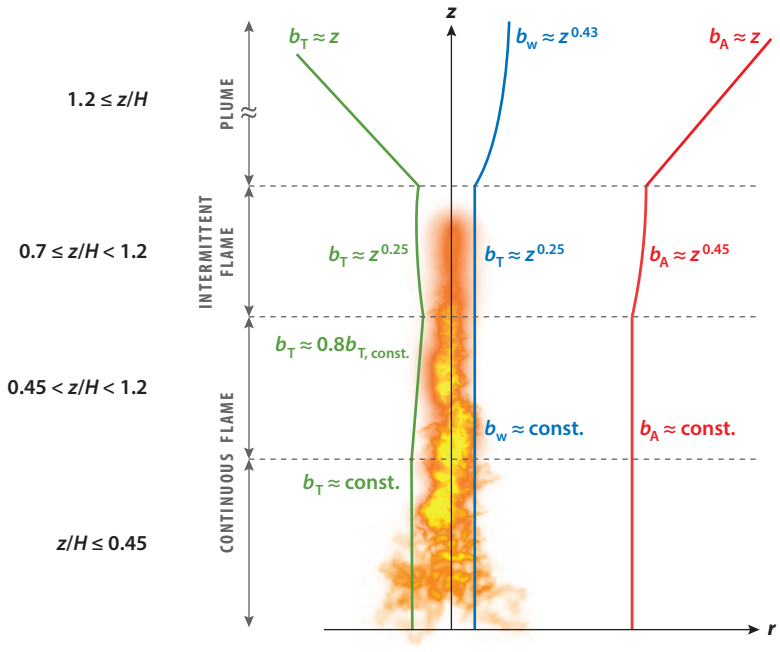

Figure 7

Schematic of different regions identified along the axial z and radial r directions. According to Lei et al. (2015b), for all fire sizes, on average, the radius based on axial velocity (b_A) is greater than the radius based on the excess temperature (b_T), which itself is greater than the radius based on the azimuthal velocity (b_w), that is throughout the height of a fire whirl $b_A > b_T > b_w$.

in fire whirls is far greater than that of pool fires in a quiescent environment. The intermittent region usually occurs at $0.7 \leq z/H < 1.22$, where $z/H = 1.22$ corresponds to the luminous tip of the fire whirl. Velocity fluctuations are significant within this region, and the centerline axial velocity decreases rapidly. Next, the plume region extends beyond the visible tip of the whirl core, where the axial velocity decelerates to the ambient flow. Customarily, the plume behavior is characterized based on flow conditions at its virtual origin (Morton et al. 1956, Turner 1979, Hunt & Kaye 2001). The location of the virtual origin within the whirling column of a fire whirl has not yet been measured or discussed. Instead, a vertical distance that is adjusted by the maximum flame height at the intermittent region (H_{if}) has been used to characterize the flow's attributes. Lei et al. (2015b) formulated this length scale as $L_v = (z - H_{if})/H$.

4.2.2. Along the *r* direction. An accurate description of the fire whirl's inner structure is intimately tied to a proper description of the whirl core and plume radius. To this end, one obtains the mean plume buoyancy and width by extending classic plume theory (Morton et al. 1956, Turner 1979) to experimental measurements of fire whirls (Emmons & Ying 1967). Adopting the standard entrainment assumption for flow in an unstratified environment where the Boussinesq approximation is applicable, and following the notation of Hunt & Kaye (2001), one can write the fluxes for a quasi-steady 3D axisymmetric fire whirl as

$$Q = 2\pi \int_0^\infty \rho U_z r \, dr, \qquad M = 2\pi \int_0^\infty \rho U_z^2 r \, dr, \qquad F = 2\pi \int_0^\infty (\rho_0 - \rho) g U_z r \, dr, \qquad 8.$$

where Q, M, and F are the mass, axial momentum, and buoyancy fluxes along the z direction, respectively, and ρ_0 is the reference density. Similar to Tohidi & Kaye (2016), Q, M, and F can be written in the form of specific fluxes as $\hat{Q} = Q/(2\pi\rho_0)$, $\hat{M} = M/(2\pi\rho_0)$, and $\hat{F} = F/(2\pi\rho_0)$ (Lee & Chu 2012). One can map the conservation equations with these specific fluxes and integrate them using the standard entrainment model that is incorporated with the fire whirl radius b_A and the mean plume buoyancy force per unit volume $\Delta\gamma$, which can be shown as

$$b_A = \hat{Q}/\sqrt{\hat{M}} \tag{9.}$$

and

$$\Delta\gamma = \frac{\rho_0 \hat{F}\hat{Q}}{\hat{M}}\chi^{-1}. \tag{10.}$$

The standard entrainment model only couples the radial variations of the inflow with shearing effects due to the axial velocity. Thus, more sophisticated entrainment models are needed. Moreover, unlike other studies (Emmons & Ying 1967, Lei et al. 2015b), Equation 9 does not require the top hat assumption for the axial velocity profile, which effectively decouples the flame length from the flow structure (Kuwana et al. 2011). In Equation 10, $\chi^{1/2}$ can be interpreted as the density deficit length scale within or beyond the fire whirl core:

$$\chi = \frac{1}{\rho_0}\int_0^\infty \rho r \, \mathrm{d}r. \tag{11.}$$

This parameter χ may represent a length scale in the radial direction within which the total density deficit accumulates, although to the authors' best knowledge, it has not yet been discussed in the fire whirl literature.

Neglecting small viscous forces, i.e., $\mathcal{O}(\mu) \approx 0$, within the rigid body rotating core of the fire whirl and considering negligible vertical diffusion for heat and species, Emmons & Ying (1967) decoupled the azimuthal velocity from the buoyancy and axial velocity, leading to a set of ordinary differential equations in terms of U_z, U_r, b_A, and $\Delta\gamma$. With a constant entrainment coefficient, the proposed model fails to predict the growth of width with height; therefore, they used a variable entrainment coefficient. In a different approach, others define b_A as the radial distance from the whirl's vertical axis at which the local axial velocity U_z has declined to a fraction of the maximum recorded value at the same height. For the continuous flame region, this is equal to 0.5 (Lei et al. 2015b) and 0.3 (Wang et al. 2016). As Equation 9 suggests, b_A varies with height. Lei et al.'s (2015b) measurements show that, when $\dot{\mathcal{Q}} \geq 200$ kW, the whirl's upward flow is constrained by an external downward flow that makes b_A relatively constant for the first half of the continuous flame region, i.e., $z/H \leq 0.45$. Then, b_A increases in the upper half of the continuous region and even decreases with higher rates in the intermittent and plume regions. Lei et al. (2015b) observed a power law correlation of the form $b_A = 3.08\dot{\mathcal{Q}}^{0.26}$, where b_A is in centimeters and the heat release rate is in kilowatts. **Figure 7** shows spatial variations of b_A for a typical quasi-steady, on-source fire whirl.

Similarly, the temperature core radius b_T is defined as the radial location where the excess temperature declines to half of the maximum recorded value at that height (Lei et al. 2015b). Due to cyclostrophic balance, flame pulsations are suppressed in the radial direction, causing the flame radius to be relatively constant through the first half of the continuous flame region, provided that $\dot{\mathcal{Q}} > 150$ kW. Therefore, b_T is a reasonable candidate to describe the flame shape in the axial direction (Lei et al. 2015b). Beyond the first half of the continuous flame region and up to the end of the intermittent flame zone, b_T declines to a minimum that is approximately 80% of the average recorded value. This implies that a considerable fraction of convective heat is constrained and transported upward in the vortex core. After the intermittent region, b_T grows

with height (L_v). Lei et al. (2015b) also found an empirical correlation, $b_T = 2.19\dot{Q}^{0.31}$, where b_T is in centimeters and the heat release rate $\dot{Q}$ is in kilowatts. **Figure 7** shows variations of b_T with respect to height.

A qualitative comparison of b_A with b_T shows that, for the lower half of the continuous flame region, b_A is slightly smaller than b_T. This illustrates the constraining effects of the downdraft flow within the domain (Lei et al. 2015b). However, for a wide range of heat release rates, b_A is always larger than the measured b_T at the same height. This holds true along the three regions of the whirl core and implies that the axial velocity core expands faster than the temperature core.

Moreover, the mean whirl (vortex) core radius b_w is characterized such that, beyond it, the circulation is nearly constant, i.e., the tangential velocity is maximum (Lei et al. 2015b, Hartl & Smits 2016). The mean vortex core radius is correlated with the heat release rate as $b_w = 2.36\dot{Q}^{0.28}$, where b_w is in centimeters and $\dot{Q}$ is in kilowatts. Additionally, b_w is always less than b_T and b_A. With respect to variations in height, Lei et al. (2015b) observed that b_w is relatively constant for $z/L_h \leq 1.0$. From the experimental findings of Lei et al. (2015b), one can infer that, on average, $b_A > b_T > b_w$ throughout the height of the fire whirl. In addition, b_w increases with height in the intermittent and plume regions (**Figure 7**).

4.3. Velocity Field

Having defined the geometric characteristics of fire whirls, we can now describe the velocity field, which is closely related to the radial inflow boundary layer at the base.

4.3.1. Radial velocity component U_r. As the fluid particles adjacent to the solid boundary decelerate, the cyclostrophic balance between the centrifugal force and the pressure gradient generated by buoyancy and circulation is disturbed. This leads to the formation of the radial boundary layer toward the center of the whirl column (Byram & Martin 1962, 1970; Ying & Chang 1970; Muraszew et al. 1979; Hassan et al. 2005; Hayashi et al. 2011; Lei et al. 2015b). The isothermal model of Ying & Chang (1970) also shows that the maximum radial velocity occurs adjacent to the surface and reverses direction close to the upper parts of the boundary layer, indicating the presence of a circulation zone (Hartl & Smits 2016). Additionally, other PIV measurements (Hassan et al. 2005) show that outside of the whirl core, the radial velocity rises to a maximum value that is smaller than the tangential and axial velocity at the same heights. On this note, the maximum radial velocity is linearly correlated with circulation (Ying & Chang 1970, Hartl 2016). Hartl & Smits (2016) reported that the recirculation region thickness near the base extends up to 15 mm above the fuel (burner) surface for all combinations of the burning rate and ambient circulation. Within this region, the magnitude of the average radial velocity is considerable for both pool and burner fire beds, although it drastically reduces to negligible values for $z > 15$ mm. **Figure 6*b*** shows a typical distribution of the radial velocity in the r direction.

4.3.2. Azimuthal velocity component U_θ. Given the variations of b_w with respect to the height and heat release rate, the maximum azimuthal velocity $U_{\theta_{max}}$ tends to increase between $0 \leq z/L_h \leq 1.25$ and decrease beyond $z/L_h = 1.25$ (Lei et al. 2015b). After this region, the rate of decline of $U_{\theta_{max}}$ is reported to be equal for all fire loads. In the continuous flame zone, $U_{\theta_{max}}$ correlates with heat release rate as $U_{\theta_{max}} = 1.58\dot{Q}^{0.22}$. Despite these variations, the normalized azimuthal velocity profile $U_\theta / U_{\theta_{max}}$ with respect to the normalized radial distance r/b_w is self-similar, with insignificant scatter around the Burgers vortex model (**Figure 6*a***). This is true for a wide range

of $\dot{Q}$ and at any height (Byram & Martin 1970, Hassan et al. 2005, Akhmetov et al. 2007, Hartl & Smits 2016, Wang et al. 2016).

4.3.3. Axial velocity component U_z. With specific fluxes, the axial velocity above the boundary layer can be obtained by $U_z = \hat{M}/\hat{Q}$. Alternatively, by coupling circulation and buoyancy, Lei et al. (2015b) derived an analytic expression for the axial velocity that is valid for $z \geq \delta_r$:

$$\frac{\partial U_z^2}{\partial z} = \frac{2(T_{\text{C.L.}} - T_\infty)}{T_\infty} g + \frac{\partial}{\partial z}\left[\frac{U_\theta^2}{2}\left(\frac{1}{\eta_1} + \frac{\rho_\infty}{\rho}\frac{1}{\eta_2}\right)\right], \qquad z \geq \delta_r, \tag{12.}$$

where $T_{\text{C.L.}}$ is the centerline temperature, δ_r is the thickness of the radial boundary layer at the base, and η_1 and η_2 are exponents of power law fits of the azimuthal velocity distribution in the radial direction through the solid body rotating core and the free vortex zone, respectively. Because Equation 12 is valid for $z \geq \delta_r$, it can be integrated from δ_r to any height to give the excess axial velocity, i.e., $(U_z^2 - U_{z|\delta_r}^2)_{|r=0}$. Equation 12 indicates that, in fire whirls, the centerline axial velocity depends not only on buoyancy, but also on the radial distribution of the azimuthal velocity (circulation). Hence, within the fire whirl core, vorticity, temperature, and axial velocity are all coupled (Lei et al. 2015b).

Zhou & Wu's (2007) experiments have shown that at various levels, the circulation in fire whirls causes an initial reduction of the centerline axial velocity compared to nonswirling pool fires with the same source characteristics due to the formation of a viscous region in the boundary layer. Hence, the fire whirl's flame in the continuous region consists of both a viscous region and a buoyancy-dominated inviscid region. Lei et al. (2015b) also observed this and found that the axial centerline velocity varies with height as $U_{z|r=0} \sim z^{1/3}$ within the continuous flame region and $U_{z|r=0} \sim z^{-2/3}$ throughout the intermittent region before the fire whirl decelerates back to the plume zone. Consistent with buoyancy-dominated flows in which inertia is balanced by buoyancy (Thomas 1963), Hartl & Smits (2016) argued using dimensional analysis that the centerline axial velocity in the continuous flame region of fire whirls scales as $z^{1/2}$ and that, as the height increases to the plume region, fire whirls behave more like a buoyant plume with a weak swirl rather than a strong swirling jet. On this matter, one can calculate the expansion rate of the fire whirl plume from the axial velocity, the azimuthal velocity, and the excess temperature. However, the stabilizing effects of circulation deliver smaller expansion rates relative to the swirling jets ejected to the quiescent ambient (Section 5.4) (Beér & Chigier 1972). As the axial velocity decelerates to the plume region, the radial density stratification and consequently the cyclostrophic balance are disturbed due to the absence of the flame sheet. Thus, the influence of circulation is reduced, and subsequently, the straining effects of the vortex column decrease. This expands the fire whirl plume radius such that the faster increasing rate of b_A leads to a more rapid decay of $U_{z|r=0}$. One can better understand these processes by following the vertical variations of U_z and b_A shown in **Figure 6*c*** and **Figure 7**, respectively.

The radial distribution of axial velocity is believed to follow the temperature distribution along the r direction (Emmons & Ying 1967). Lei et al.'s (2015b) measurements have confirmed this and found that within the continuous flame region, the maximum axial velocity does not occur at the centerline axis. This suggests a hump-like distribution in the r direction. As the height increases, the hump-like profile becomes a plateau with no strict self-similar behavior between the radial profiles (Emmons & Ying 1967, Lei et al. 2015b). Through the intermittent flame zone, the plateau-like velocity profile takes a Gaussian form, with its maximum value at the centerline. Hassan et al. (2005) and Wang et al.'s (2016) PIV measurements reveal a similar Gaussian radial profile for the normalized axial velocity plotted against the normalized radius, regardless of the circulation strength and height. Additionally, Lei et al.'s (2015b) experimental

measurements suggest that the data's scatter around Gaussian fits is less in the plume region than in the intermittent flame zone (see the vertical variations of the axial velocity profile in the r direction in **Figure 6*c***).

4.4. Thermal Composition

The thermal composition of the fire whirl is closely related to its unique flow structure. The temperature distribution and influential processes on its formation are described below, along with proposed models for the radiation field surrounding the vortex core.

4.4.1. Temperature *T*. Emmons & Ying (1967) first measured the radial temperature distribution of a liquid (acetone) pool fire whirl at a single height and reported a hump-like profile in the r direction (**Figure 6*d***). This has also been seen in measurements by Lei et al. (2011, 2015b) and Wang et al. (2015). The maximum recorded temperatures occurred near/within the flame sheet, where this value was 1.6 times the centerline temperature ($T_{\max} - T_\infty \approx 1.6T_{r=0}$). This implies that the fire whirl has a fuel-rich core with no active combustion reaction (Wang et al. 2015), which significantly influences the radial temperature distribution throughout the continuous flame region (Zhou et al. 2013). The radius of this core is defined as the location where $T = T_{\max}$ (Emmons & Ying 1967). Outside this core, the temperature sharply decreases (Muraszew et al. 1979). In addition, the radial gradient of temperature decreases with increasing height due to continuous heat transfer from the reactive flame sheet to the thermal core (increase in b_T) (Lei et al. 2015b). With increasing height from the intermittent flame region and beyond, the location of maximum excess temperature shifts toward the whirl's centerline and forms a Gaussian profile regardless of the heat release rate. These Gaussian profiles within each flame region are self-similar. This suggests that the fire source dimension D_0 and heat release rate $\dot{Q}$ do not considerably affect the radial distribution of temperature at high elevations (Lei et al. 2011, 2015b; Wang et al. 2015). Moreover, the flame temperature of whirling flames has been measured to be 1.2 times that of their nonwhirling counterparts (Grishin et al. 2005). This behavior is attributed to higher diffusion rates due to a better oxygen supply in fire whirls' elongated combustion region.

Similarly, because turbulence is suppressed in fire whirls, which subsequently reduces mixing with cold ambient air throughout the free vortex column, temperature decreases slowly with height in the continuous flame region. Throughout this region, there is a correlation between excess temperature and the normalized height, i.e., $\Delta T \sim (z/H)^{-0.06}$ (Lei et al. 2015b). The exponent of temperature decay later decreases to -1.79 for the intermittent flame region. In the plume, the variation of excess temperature along the z axis (increase in L_v) scales with $z^{-5/3}$ (Mullen & Maxworthy 1977, Lei et al. 2011), which is consistent with classic observations for nonrotating turbulent plumes. Additionally, Lei et al. (2015b) showed that there is a power law correlation between the excess temperature decay and L_v, where the fitted exponent varies between -1.51 and -0.09 for different heat release rates at the source. This scattering can be attributed to different turbulent dissipation rates within the plume region. Wang et al. (2015) also reported these trends, yet with slightly different exponent values.

4.4.2. Radiation. To evaluate the radiative heat flux from fire whirls to the external surroundings, researchers have often assumed the whirl to be a homogeneous black body emitter (Zhou et al. 2011), similar to studies from pool fires (Hamins et al. 1996). Zhou et al. (2011, 2014) have proposed two models that show that there is a considerable variation in the radiant heat flux profile as height increases. In fire whirls with various pool sizes, the radiative heat flux increases throughout the continuous flame zone up to $z/H = 0.4$ and then decreases rapidly beyond it

(Zhou et al. 2011, Wang et al. 2015). The decline of radiative heat flux in the plume region is faster than in the intermittent zone, similar to nonswirling pool fires, where the corresponding height through which the radiative heat flux increases is up to $z/H = 0.5$ (Hamins et al. 1996). As expected, it is reported that the radiative heat flux decreases monotonically in the radial direction.

5. GOVERNING PROCESSES

Based on the influential parameters described in Section 2, researchers have established scaling laws to describe some of the underlying processes that govern the structure of quasi-steady, on-source fire whirls, which are reviewed below.

5.1. Circulation

Circulation is, indeed, the major factor that distinguishes fire whirls from nonswirling fires. Variations in temperature, height, and the velocity field (in particular, the axial velocity) are directly interrelated with circulation. In this regard, one finds using dimensional analysis that the axial velocity and temperature scale with the fire power P. This is analogous to the (virtual) point source in turbulent plumes, and it implies that $U_z \sim P^{1/3}$ and $\Delta T \sim P^{2/3}$ (Mullen & Maxworthy 1977). The imparted power into the system has a direct relationship with buoyancy as $\hat{F} = (Pg)/(\rho_0 C_p T_\infty)$, given that temperature localization is allowed (Lee & Chu 2012). Using the same analysis, Mullen & Maxworthy (1977) found that the vortex core diameter D_w varies linearly with the core Reynolds number Γ/ν and the boundary layer thickness δ_r. Mullen & Maxworthy (1977) and Hartl & Smits (2016) have also shown that the circulation is independent of height. The fire whirl core structure varies sporadically, but due to constant circulation strength, the outer flow apparently adjusts and sustains itself in the vertical direction relative to the core behavior (Mullen & Maxworthy 1977).

Considering circulation effects on the axial velocity, McCaffrey (1979) found that, in a general nonswirling pool fire, the Froude number based on the axial velocity is constant. However, this is not the case for fire whirls, as Zhou et al. (2011) argued that both buoyant plume theory and the circulation-induced vortex should be included in the dimensional analysis. According to Zhou et al. (2011), Fr is approximately $(\Gamma/\sqrt{gz^3})^\eta$, where η is found to be 0.22 through the continuous flame region and 0.77 through the plume. However, this scaling seems to be inappropriate because the circulation in the free vortex region is typically constant along the vertical direction (Lei et al. 2011, Hartl & Smits 2016). Hartl & Smits (2016) defined the Froude number based on the centerline axial velocity as $U_{z|r=0}/\sqrt{gz}$ and assumed that Fr and circulation are independent of height. Dimensional analysis of their PIV results led to $Fr = 1.65(\dot{\mathcal{Q}}^* L_h^*)^{-0.18}$, where $L_h^* = L_s/D_c$ is the normalized horizontal length scale, L_s is the gap size in their half-cylinder setup, and D_c is the diameter of the cylinders. Hartl & Smits (2016) showed that this Froude number becomes invariant to large values of $\dot{\mathcal{Q}}^* L_h^*$. Therefore, the centerline axial velocity is independent of $\dot{\mathcal{Q}}^* L_h^*$, i.e., $U_{z|r=0} \sim z^{1/2}$, as mentioned in Section 4.3.3.

Kuwana et al.'s (2011) experiments examined the influence of circulation strength on the fire whirl's burning rate and flame height and applied weak and strong circulations to both burner and pool-source fire whirls. Given that the diameter of the burner and the pool source were the same (0.3 cm), Kuwana et al. (2011) found that strong circulation increases the burning rate and flame height in both pool and burner fire whirls. However, weak circulation only increased the burning rate of the pool source up to three times the original value and did not significantly change its flame height. This is due to the constant burning rate in the burner fire whirl, whereas in the pool fire whirl, even a slight circulation increases the heat feedback from the flame sheet to the fuel surface at the base and subsequently increases the burning rate.

Low–Rossby number fire whirls, namely those with high circulation, are believed to be rotation controlled. Chuah et al. (2011) examined this for inclined fire whirls on a slope under strong circulation. The experimental evidence suggests that low–Rossby number fire whirls are dominated by rotation ($Ro \ll Fr$) in that buoyancy contributes less to the flow structure. Additionally, a linear correlation is found between H/D_0 and $Pe/(16f)$, where f is the stoichiometric mass ratio of fuel to air. This implies that the flame height H is independent of the inclination angle and buoyancy. In addition, viscous core effects on the outer regions were incorporated in an analytic model developed by Chuah et al. (2011), which Klimenko & Williams (2013) later expanded by employing the strong vortex approximation and its compensating regime. Although the analytical model is decoupled from density stratification throughout the domain, it shows that the entrainment flow in low–Rossby number fire whirls approaches the compensating regime, which is not best described by the Burgers vortex model (Klimenko 2014). As a result, any change in U_z and U_r (the flow structure) triggers changes in the mixture fraction, leading to variations in the flame height. The far-field asymptotic solutions of Klimenko & Williams' (2013) model agree well with experimental data. Further, Zhou et al. (2016) documented nine flame patterns that resulted from the change in external circulation strength and heat release rate of buoyant diffusion flames in a rotating screen setup. As circulation (angular velocity of the screen) increased, flames transitioned from a free buoyant flame to one that was inclined and finally to a fire whirl; however, even after this transition, the whirl continued to transition to different shapes until it finally became irregular and extinguished. Using a two half-cylinder experimental setup where circulation is not mechanically generated, Hartl & Smits (2016) found that beyond the entrainment zone at the base, circulation may be dependent on mass entrainment for stoichiometric combustion.

5.2. Height

Relative to nonswirling fires, the most conspicuous feature of fire whirls is the increase in flame height, where a 10-fold (Emmons & Ying 1967) to 30-fold (Battaglia et al. 2000b) increase in height has been documented. A major cause of this increase is related to the intensified burning rate (Chuah & Kushida 2007), due to increased heat transfer at the fuel surface, and to circulation, which modifies entrainment and mixing. Chigier et al. (1970) and Battaglia et al. (2000a) have found the flame height to increase with applied circulation even when the burning rate and the fuel source diameter D_0 are constant. Kuwana et al. (2008) used scaling analysis to describe this relationship:

$$\frac{H}{D_0} \sim \begin{cases} \left(\frac{\Gamma^2}{gD_0^3}\right)^{1/3} & \text{for} \quad \frac{\Gamma^2}{gD_0^3} \to \infty \\ \left(\frac{\Gamma^2}{gD_0^3}\right) & \text{for} \quad \frac{\Gamma^2}{gD_0^3} \to 0 \end{cases}. \qquad 13.$$

In Equation 13, very large values of $\Gamma^2/(gD_0^3)$ correspond to small pool fires, whereas very small values correspond to large pool fires. Equation 13 asymptotically converges to simulation results of Battaglia et al. (2000b) as $\Gamma^2/(gD_0^3)$ increases. This suggests that, for small fire whirls, the flame height is circulation controlled, whereas for large fire whirls other parameters such as the burning rate and the buoyancy are also important. Chow et al. (2010) also established a positive correlation between the fire whirl height and the product of the dimensionless fire power $\dot{Q}^*$ and pool diameter D_0: $H = 3.59\dot{Q}^{*2/5}D_0$.

Byram & Martin (1962) and Lei et al. (2011) have argued that the flame radius in the continuous flame region is nearly equal to that of the vortex core above the radial boundary layer (Byram & Martin 1962; Lei et al. 2011). Given this, and assuming that the flame has a quasi-steady axisymmetric state with constant ambient circulation in the axial direction that follows the

Burgers vortex model, one obtains a power law relation $b_w \sim (HD_0^{\eta})/\Gamma$, where η is a fitting exponent. The inverse relationship of b_w with circulation is in agreement with the results of Battaglia et al.'s (2000b) inviscid model. Considering discussions on the turbulence suppression mechanism (Section 5.4) and following the scaling expression for the vortex core radius, one can infer that the fire whirl height is a function of both the burning rate and circulation. This is evident in the result of dimensional analysis, $H = \mathcal{G} D_0 (\dot{\mathcal{Q}}^* \Gamma^{*2})^{\eta_m}$, in which $\dot{\mathcal{Q}}^*$ is the dimensionless fire power (Section 2), $\Gamma^* = \Gamma/\sqrt{g D_0^3}$, and η_m and $\mathcal{G}$ are empirically obtained variables (Lei et al. 2011). These results agree with measurements by Emmons & Ying (1967). Based on these results, one can obtain a flame height expression $H = \Gamma^{*\eta_S(2+\eta_m)} D_0^{1+3\eta_S(\eta_m-1)/2}$, where for laminar fire whirls η_m and η_S are 0.5 and 0.4, respectively (Lei et al. 2012). For turbulent boundary layers at the base, these values change to 1 and 1/3, respectively. The results are consistent with Emori & Saito's (1982) observations for laminar fire whirls and appear to hold true prior to the formation of any vortex breakdown. Zhou et al. (2013) also proposed that if one normalizes the fire whirl's flame height with the flame height of a similar nonswirling fire, there is a linear correlation in the logarithmic space between the normalized heights and circulation. Further, based on PIV measurement results, Hartl & Smits (2016) proposed a scaling relationship $H = 0.7 D_0 \Gamma^{*1.11}$, which implies that circulation is the dominant parameter determining a fire whirl's height. These results appear to provide a better fit to the experimental data than the correlation Kuwana et al. (2008) proposed.

5.3. Boundary Layer and Burning Rate

As previously mentioned, the presence of drag (friction) at the base is crucial for fire whirl formation. Previous studies by Morton (1970), Emmons & Ying (1967), and Dobashi et al. (2015) suggested that disruption of the cyclostrophic balance at the base and formation of an Ekman-type inflow boundary layer due to viscous effects change the flame shape such that the heat and mass transfer rates on the fuel surface (i.e., the burning rate) increase significantly in relation to nonwhirling fires or whirling flames without viscous effects at their base (**Figure 8*b***). This is consistent with the Ekman-layer solution on a solid surface, where the balance between circulation, pressure gradient, and friction (drag) force within the boundary layer delivers a velocity component toward the low pressure zone, i.e., radial inflow (Kundu et al. 2004). In fire whirls, the behaviors of the boundary layer, circulation, and burning rate are all interrelated. In a set of pool fire whirl experiments, Lei et al. (2012) observed that the fuel surface often oscillates slightly due to flame wander and the presence of unstable secondary flows. In relatively large fire whirls, circular ripples are continuously generated and move toward the center of the liquid fuel surface due to the strong inflow at the boundary layer. Moreover, as the height of ripples increases, these wave-like structures approach the center. In rare cases, with relatively strong circulation, Lei et al. (2012) reported that the ripples abruptly break into sprays in the center and evaporate through the high temperature core. Under strong circulation, liquid fuel can be directly sucked into the vortex core, and in the case of solid combustible materials, this may lead to a firebrand shower and subsequent spot fire ignitions, as solid fuels have much slower pyrolysis rates than liquid fuels (Lei et al. 2012). With regard to these observations, it can be concluded that, although the dynamics of these complex interactions is not fully understood, collectively, they may enhance the fuel evaporation rate (Lei et al. 2012).

Previous studies have reported a dramatic increase in the fire whirl's burning rate for wildland (solid) fuels, 1.4–4.2 times the original burning rate of a nonwhirling fire (Martin et al. 1976). Emmons & Ying's (1967) pioneering study of an acetone pool fire whirl also showed that the mass

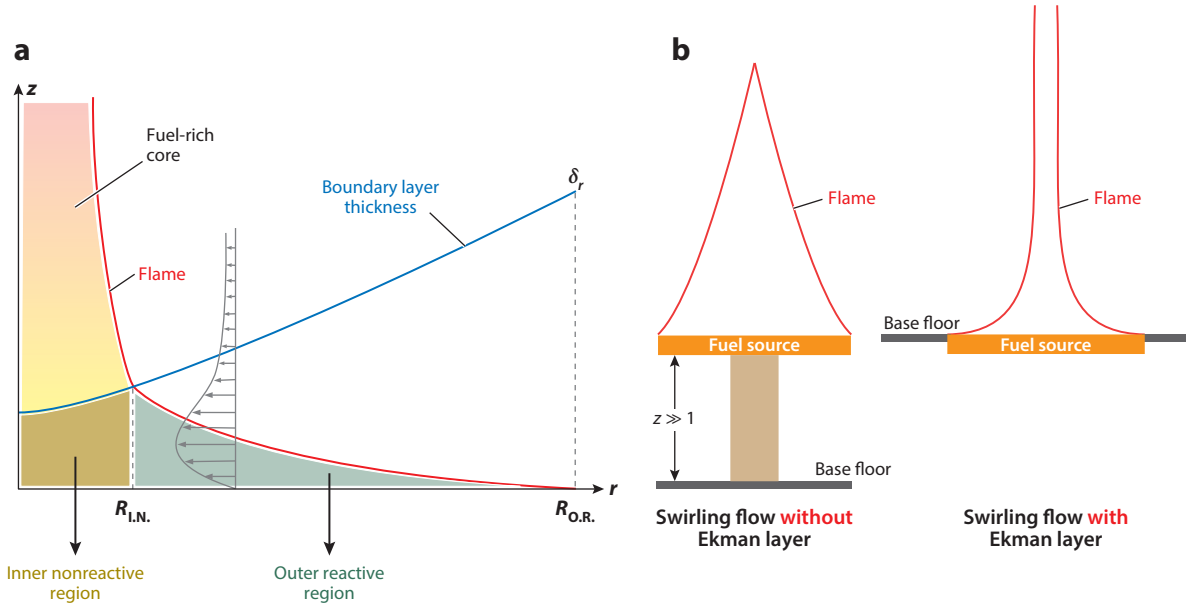

Figure 8

(*a*) Schematic showing the different regions within the boundary layer at the base of a fire whirl (Lei et al. 2012). (*b*) Viscous effects of the Ekman boundary layer on the flame shape at the base of a fire whirl (Dobashi et al. 2015).

loss rate increases monotonically with increasing ambient circulation. Following the discussion above, heat transfer at the fuel surface was thought to increase significantly due to the flow structure (presence of swirl), effectively increasing the heat transfer coefficient for fire whirls (Muraszew et al. 1979). In larger fires, the radiative heat feedback fraction was found to increase for fire whirls compared to that of pool fires (Zhou et al. 2011). However, Snegirev et al. (2004) found that this fraction decreases slightly with circulation. This indicates that the increase in the burning rate is still due to enhanced air entrainment through the Ekman-type boundary layer adjacent to the fuel surface.

Interestingly, Chuah et al. (2009) found that the diameter D_w of the vortex core increases inversely with the diameter of the fuel surface (Chuah et al. 2009). Following this observation, Lei et al. (2012) argued that the inflow boundary layer can be separated into an inner nonreactive region, $r \leq R_{I.N.}$, and an outer reactive region, $R_{I.N.} < r \leq R_{O.R.}$ (**Figure 8*a***). The mechanisms of heat and mass transfer within these regions are considerably different. Dobashi et al. (2015) showed experimentally that viscous effects near the surface (the Ekman layer) cause the flame base to approach the fuel surface, increasing heat transfer and the burning rate. Given this, the estimate of the burning rate in a laminar boundary layer will be different from that of a turbulent one. For turbulent boundary layers with $Pr \approx 1$, convective heat transfer on the fuel surface can be related to the wall friction by an extension of the Chilton–Colburn analogy (Rotta 1964, Bergman et al. 2011). In fire whirls with laminar boundary layers, the Chilton–Colburn analogy is not appropriate, because there is a large radial pressure gradient. However, Glassman et al. (2014) showed that, for a laminar convective burning problem, the mass loss rate per unit area can be approximated by stagnant film theory, using a radiation correction from Fineman (1962). Given these, integration of the momentum equations for turbulent and laminar boundary layers results in the total mass loss rate in fire whirls, $\dot{m} = \mathcal{G}\Gamma^{1/(\eta_m+1)} R_{O.R.}$, where $\mathcal{G}$ is a function of various

parameters including the entrainment coefficient (Lei et al. 2012). For laminar boundary layers, one finds that $\eta_m = 1$, whereas for turbulent cases η_m depends on the surface roughness, which varies between 1/7 and 1/4. Results of these semi-empirical expressions compare well with the experimental data of Emmons & Ying (1967) and Lei et al. (2012).

5.4. Vortex Breakdown, Turbulence Suppression, and Entrainment

The flow structure of a quasi-steady, on-source fire whirl is primarily formed and sustained by its unique entrainment mechanism, which in turn can be affected by phenomena such as vortex breakdown and turbulence suppression. In Emmon & Ying's (1967) theory, the mixing coefficient decreases with increasing circulation strength. This suppresses molecular entrainment of oxygen from the ambient to the vortex core and results in flame elongation. They observed that the spiral rise of fluid in the core is surrounded by a rapidly rotating free vortex that generates surface waves on the core that move with $U_{\text{wave}} = \Gamma/(4\pi b_{\text{w}})$. Analogous to a hydraulic jump, if the fire whirl core travels faster or slower than U_{wave}, it corresponds to shooting or tranquil flow, respectively. This is particularly the case once vortex breakdown occurs. It is important that turbulence suppression damps the effective entrainment of air into the vortex core through the part that is from above the boundary layer up to the intermittent flame zone (Lei et al. 2015b). However, the presence of vortex breakdown, which is accompanied by high turbulence and circulation, accounts for the highly effective entrainment in the plume region as well as the growth of b_{w} beyond the intermittent flame zone. High circulation, which may lead to vortex breakdown, increases the inflow rate and subsequently the entrainment through the boundary layer thickness (Zhou et al. 2013). Zhou et al.'s (2013) experimental results suggest that air entrained through the boundary layer is sufficient for sustained complete combustion. Moreover, they found that, above the boundary layer thickness and through the flaming region, the (dimensionless) mass flow rate gradually rises and drastically increases in the vertical direction. Eventually, the mass flow rate decays in the plume region. Hence, several entrainment zones can be identified along the fire whirl height (Zhou et al. 2013). In Lei et al.'s (2015b) experiments, variations of the mass flow rate with height show that the entrained air through the inflow boundary layer is often not sufficient for stoichiometric combustion of the fuel, even though the air and fuel are relatively well mixed. Nonetheless, $\dot{m}$ varies considerably through the height, consistent with the results of Zhou et al. (2013). As a result, fire whirls consist of a laminarized zone at a lower height that coexists with turbulent regions at increasing heights. This notion justifies the highly suppressed entrainment within the continuous flame region and appreciable mixing through the plume region (Zhou et al. 2013, Lei et al. 2015b).

Chigier et al. (1970) documented a considerable reduction due to turbulence suppression of mixing and entrainment along swirling jet flames. In quasi-steady, on-source fire whirls where the flame core radius remains relatively steady, mixing is quite different from pool fires, where this radius varies significantly as a function of time, due to intermittent puffing of the flame (Tieszen 2001). Therefore, the flow field of a fire whirl can be described as an inner fuel-rich jet within a coaxial stream with swirl, through which the entrained air gradually mixes with the fuel in the flaming region (Lei et al. 2015b). As a result, one can identify two turbulent suppression mechanisms to describe such behavior. The first mechanism is due to a radial force balance, where the radially outward centrifugal force is equal to the radially inward pressure gradient ($\partial p/\partial r \sim \rho U_\theta^2/r$). This so-called cyclostrophic balance, which suppresses the transverse motion of fluid particles in the radial direction, leads to a reduction in turbulent mixing along the vortex core height. From a different perspective, others (Beér & Chigier 1972) attribute the suppression in mixing to a reduction of shear stresses at the vortex core interface. Regardless of the cause, this mechanism can be quantified by introducing a simple Richardson number as $Ri_{\text{A}} \sim (U_{\theta,\max}/U_{z,\max})^2$

(Lei et al. 2015b). The proposed Richardson number is analogous to the swirl number that is used to characterize the circulation strength in swirling jets (Ellison & Turner 1959). The larger the value of Ri_A, the more intense the turbulence suppression becomes.

The second mechanism results from stable stratification in the radial direction (Lei et al. 2015b). In fact, both the density gradient and the centrifugal acceleration are radially outward (Ellison & Turner 1959). Hence, contrary to the role of buoyancy in increasing mixing through the gravity field, this stable stratification reduces turbulent fluctuations and subsequently mixing at the vortex core interface in the r direction. These effects can be quantified by $Ri_B = (\Delta\rho_m/\rho_\infty)(U_{\theta,\max}/U_{z,\max})^2$ (Lei et al. 2015b). The greater the value of Ri_B, the more the turbulent mixing is suppressed. Further, Lei et al. (2015b) showed that the entrainment coefficient α and Ri_B are inversely proportional. This is comparable to the turbulent mixing regime, due to the coexistence of intermittent vortex mixing and continuous entrainment along the cusp of the fire whirl core (Christodoulou 1986).

5.5. The Blue Whirl

Recent experiments have revealed an exciting new phenomenon described as the blue whirl. Using a conventional fire whirl setup similar to that of **Figure 4*a***, Xiao et al. (2016) observed a traditional fire whirl that underwent what is thought to be a bubble mode of vortex breakdown. The major modification between this setup and previous experiments was that it was formed over a water surface that provided a smoother boundary and emphasized the effects of the radial boundary layer on the flame structure. The resulting flame (**Figure 1*d***) consists of a light blue cone at the base, a bright ring, and a purple haze above.

One of the most fascinating aspects of this flame is that, once transitioned, it burned without any yellow flame, indicating soot-free combustion, even when directly burning *n*-heptane, which is usually a sooty fuel. Two physical mechanisms were speculated to be important for the formation of a blue whirl: vortex breakdown and fast mixing. As a yellow fire whirl is formed, it is seen to transition to what resembles a bubble mode vortex breakdown with a stagnation point and recirculation zone at the core of the vortex. During the transition, this could be visualized with soot remaining from a yellow whirl entraining into the recirculation zone of the blue whirl. Fast mixing rates are expected that may favor soot-free combustion, similar to effects seen in highly strained coflow or opposed-jet diffusion flames (Lin & Faeth 1996a,b).

Many questions still remain as to the source of and processes occurring during transition and steady burning of a blue whirl. For instance, measurements or simulations of the flow field during the transition process or steady burning have not yet been completed, so we do not yet have a complete understanding of the fluid dynamic processes.

6. CONCLUSIONS AND FUTURE DIRECTIONS

Despite many years of study, fire whirls continue to fascinate the scientific community and present challenges for fire safety. Without a definitive theory of the flow structure for a fire whirl, many gaps in our understanding remain. Much progress has been made on on-source, quasi-steady fire whirls, such as those formed in enclosed laboratory apparatuses. However, some open questions remain. First and foremost, the underlying process governing entrainment is not well known. In Emmons & Ying's (1967) early work, they raised clear issues with regard to the treatment of entrainment as a function of height, and although some detailed PIV measurements have assisted in this understanding, these issues have not yet been fully resolved. This will help researchers better formulate a model of the fire whirl.

Other types of fire whirls continue to challenge our understanding, particularly those that occur off source or are nonsteady. Certainly the velocity and temperature fields within these whirls may differ, but exactly how remains to be seen. A reliable method for generating these whirls within the laboratory, as well as detailed measurements of their structures, would be very beneficial to our understanding. Even stationary fire whirls over a fuel source precess around the source, causing them to move and wander, triggering unknown effects to the structure of the fire whirl, especially when they are near the limits of their stability (e.g., fuel rich or high swirl). The effects of the level of circulation (e.g., Rossby number) on the structure of fire whirls are not well known, as most experiments have been performed only under a limited range of circulations and scales.

Scaling laws that describe the formation of these complex whirls have highlighted the dependence on ambient cross flow; however, there is no general form that describes the conditions for the generation of a fire whirl. This knowledge would certainly be useful in the operational modeling of wildfires, where resolutions are too coarse to resolve the complicated flow dynamics leading to fire whirls, but predictions of critical conditions could be used to send a warning to firefighters who might be dangerously near potential fire whirl formation. Still, scale modeling between laboratory wind tunnels and large-scale observations has been relatively successful in predicting the limiting conditions under which wind-driven fire whirls will form. As large-scale measurements of the fire whirl structure are, for the most part, not available, it is not yet known how this may change with increasing scale. Further measurements or numerical modeling should be performed to better understand whether the mechanisms governing the structure of fire whirls change at increasing scales.

Compared to related areas of fluid dynamics including combustion and fire phenomena, the use of numerical modeling has been relatively lacking in this field; this may be due to the complex interactions that occur during the generation and growth of a fire whirl. However, numerical models could provide invaluable information if validated against experimental measurements. Continued development of these models, particularly for cases other than stationary, on-source fire whirls, is highly encouraged. This may also be useful in understanding the formation of fire whirls, especially under wind, allowing researchers to visualize flow structures that cannot be easily measured experimentally.

The prospect of efficient combustion, highlighted by the discovery of the blue whirl, also presents many opportunities for fire whirl research. If fuel spills could be removed with significantly reduced emissions (e.g., minimal soot), it may be much easier to mitigate the hazardous consequences of oil spills. Even if blue whirls cannot be formed at this scale, traditional fire whirls produce higher mass loss rates of fuel, burn at higher temperatures, and have been observed to entrain liquid fuel at their center, all of which may be favorable for fuel spill remediation. Energy production in unique environments may also benefit from this efficient configuration, although precise control of the process will be vital to its practical implementation. Scientifically, the blue whirl and its transition from fire whirls may present an interesting platform from which to learn about the phenomenon of vortex breakdown and the formation of soot from different fuel sources.

DISCLOSURE STATEMENT

The authors are not aware of any biases that might be perceived as affecting the objectivity of this review.

ACKNOWLEDGMENTS

The authors gratefully acknowledge Sriram Bharath Hariharan for performing experiments displayed in several figures and both him and Ajay Vikram Singh for their contributions to our

understanding of the blue whirl. The authors would also like to thank Forman Williams, Antonio Sanchez, Alexander Smits, Katie Hartl, and Elaine Oran for interesting discussions that improved this manuscript. Support for this work came from the National Science Foundation awards CBET-1507623 and CBET-1554026, and from the collaborative agreement 13-CS-11221637-124 from the National Fire Decision Support Center and the USDA Forest Service Missoula Fire Sciences Laboratory. Any opinions, findings, conclusions, or recommendations expressed in this material are those of the author(s) and do not necessarily reflect the views of the National Science Foundation or the USDA Forest Service.

LITERATURE CITED

Akhmetov DG, Gavrilov NV, Nikulin VV. 2007. Flow structure in a fire tornado-like vortex. *Dokl. Phys.* 52:592–95

Albini FA. 1984. Wildland fires: Predicting the behavior of wildland fires—among nature's most potent forces—can save lives, money, and natural resources. *Am. Sci.* 72:590–97

Batchelor GK. 1953. *The Theory of Homogeneous Turbulence*. Cambridge, UK: Cambridge Univ. Press

Batchelor GK. 2000. *An Introduction to Fluid Dynamics*. Cambridge, UK: Cambridge Univ. Press

Battaglia F, McGrattan KB, Rehm RG, Baum HR. 2000a. Simulating fire whirls. *Combust. Theory Model.* 4:123–38

Battaglia F, Rehm RG, Baum HR. 2000b. The fluid mechanics of fire whirls: an inviscid model. *Phys. Fluids* 12:2859–67

Beér JM, Chigier NA. 1972. *Combustion Aerodynamics*. London: Appl. Sci.

Beér JM, Chigier NA, Davies TW, Bassindale K. 1971. Laminarization of turbulent flames in rotating environments. *Combust. Flame* 16(1):39–45

Bergman T, Incropera F, DeWitt D, Lavine A. 2011. *Fundamentals of Heat and Mass Transfer*. Hoboken, NJ: Wiley. 7th ed.

Bödewadt U. 1940. Die Drehströmung über festem Grunde. *Z. Angew. Math. Mech.* 20:241–53

Burgers JM. 1948. A mathematical model illustrating the theory of turbulence. *Adv. Appl. Mech.* 1:171–99

Byram GM, Martin RE. 1962. Fire whirlwinds in the laboratory. *Fire Control Notes* 23:13–17

Byram GM, Martin RE. 1970. The modeling of fire whirlwinds. *Forest Sci.* 16:386–99

Chigier N, Beér J, Grecov D, Bassindale K. 1970. Jet flames in rotating flow fields. *Combust. Flame* 14:171–79

Chow WK, He Z, Gao Y. 2010. Internal fire whirls in a vertical shaft. *J. Fire Sci.* 29:71–92

Christodoulou G. 1986. Interfacial mixing in stratified flows. *J. Hydraul. Res.* 24:77–92

Chuah KH, Kushida G. 2007. The prediction of flame heights and flame shapes of small fire whirls. *Proc. Combust. Inst.* 31:2599–606

Chuah KH, Kuwana K, Saito K. 2009. Modeling a fire whirl generated over a 5-cm-diameter methanol pool fire. *Combust. Flame* 156:1828–33

Chuah KH, Kuwana K, Saito K, Williams FA. 2011. Inclined fire whirls. *Proc. Combust. Inst.* 33:2417–24

Church CR, Snow JT, Dessens J. 1980. Intense atmospheric vortices associated with a 1000 MW fire. *Bull. Am. Meteorol. Soc.* 61:682–94

Countryman CM. 1971. *Fire whirls. . .why, when, and where*. Tech. Rep., USDA For. Serv., Washington, DC

Dessens J. 1962. Man-made tornadoes. *Nature* 193:13–14

Dobashi R, Okura T, Nagaoka R, Hayashi Y, Mogi T. 2015. Experimental study on flame height and radiant heat of fire whirls. *Fire Technol.* 52:1069–80

Donaltson CP, Sullivan R. 1960. Behavior of solutions of the Navier–Stokes equations for a complete class of three-dimensional viscous vortices. *Proc. Heat Transf. Fluid Mech. Inst., Stanford Univ., 15–17 June*, ed. DM Mason, WC Reynolds, WG Vincenti, pp. 16–30. Stanford, CA: Stanford Univ. Press

Ellison T, Turner J. 1959. Turbulent entrainment in stratified flows. *J. Fluid Mech.* 6:423–48

Emmons HW, Ying SJ. 1967. The fire whirl. *Proc. Combust. Inst.* 11:475–88

Emori RI, Saito K. 1982. Model experiment of hazardous forest fire whirl. *Fire Technol.* 18:319–27

Fineman SJ. 1962. *Some analytical considerations of the hybrid rocket combustion problem*. MScEng Thesis, Princeton Univ.

Forthofer JM, Goodrick SL. 2011. Review of vortices in wildland fire. *J. Combust.* 2011:984363
Glassman I, Yetter R, Glumac N. 2014. *Combustion*. Amsterdam, Neth.: Elsevier Sci.
Grishin AM. 2007. Effect of the interaction between fire tornadoes on their propagation. *Dokl. Phys.* 52:521–22
Grishin AM, Golovanov AN, Kolesnikov AA, Strokatov AA, Tsvyk RS. 2005. Experimental study of thermal and fire tornadoes. *Dokl. Phys.* 50:66–68
Hamins A, Kashiwagi T, Buch RR. 1996. Characteristics of pool fire burning. *Proc. Fire Resist. Ind. Fluids, Indianapolis, Indiana, 20 June 1995*, ed. GE Totten, J Reichel, pp. 15–41. West Conshohocken, PA: Am. Soc. Test. Mater.
Hartl KA. 2016. *Experimental investigation of laboratory fire whirls*. PhD Thesis, Princeton Univ.
Hartl KA, Smits AJ. 2016. Scaling of a small scale burner fire whirl. *Combust. Flame* 163:202–8
Hassan MI, Kuwana K, Saito K, Wang F. 2005. Flow structure of a fixed-frame type fire whirl. *Fire Saf. Sci.* 8:951–62
Hayashi Y, Kuwana K, Dobashi R. 2011. Influence of vortex structure on fire whirl behavior. *Fire Saf. Sci.* 10:671–79
Hunt G, Kaye NG. 2001. Virtual origin correction for lazy turbulent plumes. *J. Fluid Mech.* 435:377–96
Klimenko A. 2014. Strong swirl approximation and intensive vortices in the atmosphere. *J. Fluid Mech.* 738:268–98
Klimenko A, Williams F. 2013. On the flame length in firewhirls with strong vorticity. *Combust. Flame* 160:335–39
Kundu PK, Cohen IM, Hu HH. 2004. *Fluid Mechanics*. San Diego, CA: Elsevier Acad. 3rd ed.
Kuwana K, Morishita S, Dobashi R, Chuah KH, Saito K. 2011. The burning rate's effect on the flame length of weak fire whirls. *Proc. Combust. Inst.* 33:2425–32
Kuwana K, Sekimoto K, Minami T, Tashiro T, Saito K. 2013. Scale-model experiments of moving fire whirl over a line fire. *Proc. Combust. Inst.* 34:2625–31
Kuwana K, Sekimoto K, Saito K, Williams FA. 2008. Scaling fire whirls. *Fire Saf. J.* 43:252–57
Kuwana K, Sekimoto K, Saito K, Williams FA, Hayashi Y, Masuda H. 2007. Can we predict the occurrence of extreme fire whirls? *AIAA J.* 45:16–19
Lee JHW, Chu V. 2012. *Turbulent Jets and Plumes: A Lagrangian Approach*. New York: Springer Sci. Bus. Media
Lee SL, Garris CA. 1969. Formation of multiple fire whirls. *Symp. Int. Combust.* 12:265–73
Lei J, Liu N. 2016. Flame precession of fire whirls: a further experimental study. *Fire Saf. J.* 79:1–9
Lei J, Liu N, Lozano JS, Zhang L, Deng Z, Satoh K. 2013. Experimental research on flame revolution and precession of fire whirls. *Proc. Combust. Inst.* 34:2607–15
Lei J, Liu N, Satoh K. 2015a. Buoyant pool fires under imposed circulations before the formation of fire whirls. *Proc. Combust. Inst.* 35:2503–10
Lei J, Liu N, Zhang L, Chen H, Shu L, et al. 2011. Experimental research on combustion dynamics of medium-scale fire whirl. *Proc. Combust. Inst.* 33:2407–15
Lei J, Liu N, Zhang L, Deng Z, Akafuah NK, et al. 2012. Burning rates of liquid fuels in fire whirls. *Combust. Flame* 159:2104–14
Lei J, Liu N, Zhang L, Satoh K. 2015b. Temperature, velocity and air entrainment of fire whirl plume: a comprehensive experimental investigation. *Combust. Flame* 162:745–58
Lin KC, Faeth GM. 1996a. Effects of hydrodynamics on soot formation in laminar opposed-jet diffusion flames. *J. Propul. Power* 12:691–98
Lin KC, Faeth GM. 1996b. Hydrodynamic suppression of soot emissions in laminar diffusion flames. *J. Propul. Power* 12:10–17
Liu N, Liu Q, Deng Z, Kohyu S, Zhu J. 2007. Burn-out time data analysis on interaction effects among multiple fires in fire arrays. *Proc. Combust. Inst.* 31:2589–97
Martin RE, Pendleton DW, Burgess W. 1976. Effect of fire whirlwind formation on solid fuel burning rates. *Fire Technol.* 12:33–40
Matsuyama K, Tanaka F, Ishikawa N, Tanaka S, Ohmiya Y, Hayashi Y. 2004. Experimental and numerical studies on fire whirls. *Fire Saf. Sci.* 6:2–13
McCaffrey BJ. 1979. *Purely buoyant diffusion flames: some experimental results*. Natl. Bur. Stand. Inform. Rep. 79-1910, Natl. Bur. Stand., Washington, DC

McRae RH, Sharples JJ, Wilkes SR, Walker A. 2013. An Australian pyro-tornadogenesis event. *Nat. Hazards* 65:1801–11
Morton B. 1970. The physics of fire whirls. *Fire Res. Abstr. Rev.* 12:1–19
Morton B, Taylor G, Turner J. 1956. Turbulent gravitational convection from maintained and instantaneous sources. *Philos. Trans. R. Soc. A* 234:1–23
Mullen JB, Maxworthy T. 1977. A laboratory model of dust devil vortices. *Dyn. Atmos. Oceans* 1:181–214
Muraszew A, Fedele J, Kuby W. 1979. The fire whirl phenomenon. *Combust. Flame* 34:29–45
Nydahl JE. 1971. *Heat transfer for the Bödewadt problem*. PhD Thesis, Colo. State Univ.
Quintiere J. 2006. *Fundamentals of Fire Phenomena*. Hoboken, NJ: Wiley
Rotta JC. 1964. Temperaturverteilungen in der turbulenten Grenzschicht an der ebenen Platte. *Int. J. Heat Mass Transf.* 7:215–28
Satoh K, Yang KT. 1996. Experimental observations of swirling fires. *Proc. Am. Soc. Mech. Eng. Heat Transf. Div.: Int. Mech. Eng. Congr. Expo., Atlanta, Ga., 17–22 Nov.*, pp. 393–400. New York: Am. Soc. Mech. Eng.
Satoh K, Yang KT. 2000. A horizontal fire-whirl design scenario for engineering performance-based fire-code applications. *Int. J. Eng. Perform.-Based Fire Codes* 2:48–57
Satoh K, Yang KT, Dame N. 1997. Simulations of swirling fires controlled by channeled self-generated entrainment flows. *Proc. Int. Symp. Fire Saf. Sci., 5th, Melbourne, Aust., 3–7 March*, ed. Y Hasemi, pp. 201–12. London: Int. Assoc. Fire Saf. Sci.
Sharples JJ, Kiss AE, Raposo J, Viegas DX, Simpson CC. 2015. Pyrogenic vorticity from windward and lee slope fires. *Int. Congr. Model. Simul., Gold Coast, Aust. 29 Nov.–4 Dec.*, ed. T Weber, MJ McPhee, RS Anderson, pp. 291–97. Canberra, Aust.: Model. Simul. Soc. Aust. N.Z.
Simpson C, Sharples JJ, Evans JP. 2016. Sensitivity of atypical lateral fire spread to wind and slope. *Geophys. Res. Lett.* 43:1744–51
Snegirev A, Marsden J, Francis J, Makhviladze G. 2004. Numerical studies and experimental observations of whirling flames. *Int. J. Heat Mass Transf.* 47:2523–39
Soma S, Saito K. 1991. Reconstruction of fire whirls using scale models. *Combust. Flame* 86:269–84
Stewartson K. 1953. On the flow between two rotating coaxial disks. *Math. Proc. Camb. Philos. Soc.* 49:333–41
Thomas P. 1963. The size of flames from natural fires. *Symp. Int. Combust.* 9:844–59
Tieszen SR. 2001. On the fluid mechanics of fires. *Annu. Rev. Fluid Mech.* 33:67–92
Tohidi A, Kaye NB. 2016. Highly buoyant bent-over plumes in a boundary layer. *Atmos. Environ.* 131:97–114
Turner JS. 1979. *Buoyancy Effects in Fluids*. Cambridge, UK: Cambridge Univ. Press
Wang P, Liu N, Hartl K, Smits A. 2016. Measurement of the flow field of fire whirl. *Fire Technol.* 52:263–72
Wang P, Liu N, Zhang L, Bai Y, Satoh K. 2015. Fire whirl experimental facility with no enclosure of solid walls: design and validation. *Fire Technol.* 51:951–69
Xiao H, Gollner MJ, Oran ES. 2016. From fire whirls to blue whirls and combustion with reduced pollution. *PNAS* 113:9457–62
Ying SJ, Chang C. 1970. Exploratory model study of tornado-like vortex dynamics. *J. Atmos. Sci.* 27:3–14
Zhou K, Liu N, Lozano JS, Shan Y, Yao B, Satoh K. 2013. Effect of flow circulation on combustion dynamics of fire whirl. *Proc. Combust. Inst.* 34:2617–24
Zhou K, Liu N, Satoh K. 2011. Experimental research on burning rate, vertical velocity and radiation of medium-scale fire whirls. *Fire Saf. Sci.* 10:681–91
Zhou K, Liu N, Yuan X. 2016. Effect of wind on fire whirl over a line fire. *Fire Technol.* 52:865–75
Zhou K, Liu N, Zhang L, Satoh K. 2014. Thermal radiation from fire whirls: revised solid flame model. *Fire Technol.* 50:1573–87
Zhou R, Wu ZN. 2007. Fire whirls due to surrounding flame sources and the influence of the rotation speed on the flame height. *J. Fluid Mech.* 583:313–45
Zukoski EE, Kubota T, Cetegen B. 1981. Entrainment in fire plumes. *Fire Saf. J.* 3:107–21